JGR Solid Earth

RESEARCH ARTICLE
10.1029/2022JB023989

Using Seafloor Geodesy to Detect Vertical Deformation at the Hikurangi Subduction Zone: Insights From Self-Calibrating Pressure Sensors and Ocean General Circulation Models

K. Woods[1], S. C. Webb[2], L. M. Wallace[3,4], Y. Ito[5], C. Collins[6], N. Palmer[3], R. Hino[7], M. K. Savage[1], D. M. Saffer[4], E. E. Davis[8], and D. H. N. Barker[3]

[1]School of Geography, Environment and Earth Sciences, Victoria University of Wellington, Wellington, New Zealand, [2]Lamont-Doherty Earth Observatory, Columbia University, Palisades, NY, USA, [3]GNS Science, Lower Hutt, New Zealand, [4]Institute for Geophysics, University of Texas, Austin, TX, USA, [5]Disaster Prevention Research Institute, Kyoto University, Kyoto, Japan, [6]National Institute of Water and Atmospheric Research, Wellington, New Zealand, [7]Graduate School of Science, Tohoku University, Sendai, Japan, [8]Pacific Geoscience Centre, Geological Survey of Canada, Sidney, BC, Canada

Abstract Seafloor pressure sensor data is emerging as a promising approach to resolve vertical displacement of the seafloor in the offshore reaches of subduction zones, particularly in response to slow slip events (SSEs), although such signals are challenging to resolve due to sensor drift and oceanographic signals. Constraining offshore SSE slip distribution is of key importance to understanding earthquake and tsunami hazards posed by subduction zones. We processed seafloor pressure data from January to October 2019 acquired at the Hikurangi subduction zone, offshore New Zealand, to estimate vertical displacement associated with a large SSE that occurred beneath the seafloor array. The experiment included three self-calibrating sensors designed to remove sensor drift, which, together with ocean general circulation models, were essential to the identification and correction of long-period ocean variability remaining in the data after applying traditional processing techniques. We estimate that long-period oceanographic signals that were not synchronous between pressure sensors and reference sites influenced our inferred displacements by 0.3–2.6 cm, suggesting that regionally deployed reference sites alone may not provide sufficient ocean noise correction. After incorporating long-period ocean variability corrections into the processing, we calculate 1.0–3.3 cm of uplift during the SSE offshore Gisborne at northern Hikurangi, and 1.1–2.7 cm of uplift offshore the Hawke's Bay area at central Hikurangi. Some Hawke Bay displacements detected by pressure sensors near the trench were delayed by 6 weeks compared to the timing of slip onset detected by onshore Global Navigation Satellite System sites, suggesting updip migration of the SSE.

Plain Language Summary We use pressure sensors to estimate centimeter-level vertical motion of the seafloor due to New Zealand slow slip event activity in 2019. These tectonic events have been observed at subduction zones worldwide. They involve a similar amount of slip as fast earthquakes, but the slip occurs over longer periods of time (days to years). Seafloor pressure sensors are important to detecting and determining the location of offshore slow slip events, knowledge that contributes to our understanding of subduction zone processes, and to assessing the risk of future large earthquakes and tsunamis. Variations in ocean circulation can cause high noise levels in the pressure data compared to the tectonic signals of interest, which makes it challenging to calculate seafloor uplift or subsidence. Here we show that the deployment of a self-calibrating type of pressure sensor, along with knowledge from global models of ocean circulation, can significantly reduce the data noise levels. We estimate up to 3.3 cm of seafloor uplift occurred during a large slow slip event between March and June 2019 offshore New Zealand.

Key Points:

- Seafloor pressure data detected vertical seafloor deformation during 2019 slow slip events at the Hikurangi subduction zone
- Ocean Global Circulation Models can help with the removal of long-period (>3 month) oceanographic signals in seafloor pressure records
- Self-calibrated pressure sensors and depth-matched reference sites optimize resolution of seafloor vertical deformation

Supporting Information:

Supporting Information may be found in the online version of this article.

Correspondence to:

M. K. Savage,
martha.savage@vuw.ac.nz

Citation:

Woods, K., Webb, S. C., Wallace, L. M., Ito, Y., Collins, C., Palmer, N., et al. (2022). Using seafloor geodesy to detect vertical deformation at the Hikurangi subduction zone: Insights from self-calibrating pressure sensors and ocean general circulation models. *Journal of Geophysical Research: Solid Earth*, *127*, e2022JB023989. https://doi.org/10.1029/2022JB023989

Received 11 JAN 2022
Accepted 13 NOV 2022

Author Contributions:

Conceptualization: K. Woods, S. C. Webb, L. M. Wallace
Data curation: N. Palmer
Funding acquisition: S. C. Webb, L. M. Wallace, Y. Ito, M. K. Savage
Investigation: K. Woods, S. C. Webb, L. M. Wallace, Y. Ito, C. Collins, N. Palmer, R. Hino, M. K. Savage, D. M. Saffer, E. E. Davis, D. H. N. Barker

1. Introduction

Both deep and shallow slow slip events (SSEs) have been observed at subduction zones around the world, in a wide range of physical environments (Bürgmann, 2018; Saffer & Wallace, 2015; Schwartz & Rokosky, 2007). SSEs can release moment equivalent to that of an M > 7 earthquake, but the slip occurs at rates of millimeters to centimeters per day, and with durations of days to years. Continuous onshore Global Navigation Satellite System (GNSS) stations have provided the primary data sets to detect and resolve the distribution of slip in SSEs, but SSE slip on the shallow, offshore reaches of subduction thrusts is poorly resolved by onshore GNSS networks at most subduction margins (Williamson & Newman, 2018). SSEs play important roles in accommodating the plate

Methodology: K. Woods, S. C. Webb, L. M. Wallace, Y. Ito, C. Collins, N. Palmer, R. Hino, M. K. Savage, D. M. Saffer, E. E. Davis, D. H. N. Barker
Software: C. Collins
Supervision: L. M. Wallace, M. K. Savage
Validation: C. Collins
Writing – original draft: K. Woods
Writing – review & editing: K. Woods, S. C. Webb, L. M. Wallace, Y. Ito, C. Collins, N. Palmer, R. Hino, M. K. Savage, D. M. Saffer, E. E. Davis, D. H. N. Barker

motion budget and influence the seismic cycle by unloading or loading portions of subduction interfaces through transient slip (Avouac, 2015). For example, SSEs are thought to be involved in the triggering of several large recent megathrust earthquakes, such as the 2011 M 9 Tohoku-Oki earthquake in Japan (Ito et al., 2013, 2015; Kato et al., 2012), the 2014 M 8.1 Iquique earthquake in Chile (Ruiz et al., 2014), and the 2014 M 7.3 Papanoa earthquake in Mexico (Radiguet et al., 2016). Therefore, it is crucial to identify when and where subduction SSEs are occurring on all portions of the subduction interface (including offshore subduction thrusts), to establish the relationship between SSEs and earthquake occurrence, to quantify the role that SSEs play in the accommodation of plate motion budgets, and ultimately to incorporate these insights into seismic and tsunami hazard assessments and earthquake forecasts.

Seafloor pressure is a valuable geodetic observable for monitoring tectonic regions in marine environments, and has been used to detect vertical seafloor deformation due to magmatic processes since the late 1980s (Fox, 1990, 1993). Investigation of vertical deformation related to near-trench SSEs has been undertaken at the Hikurangi subduction zone, New Zealand (Wallace et al., 2016), Costa Rica (Davis et al., 2015), and the Japan Trench (Ito et al., 2013). Shallow SSEs have also been detected at the Nankai Trough in southwest Japan (Araki et al., 2017) and the Costa Rican margin (Davis et al., 2015) through the use of subseafloor borehole pressure measurements as a proxy for volumetric strain. Seafloor pressure sensor networks have been incorporated into the extensive, cabled, seafloor monitoring observatories in Japan (Kaneda, 2014; Kawaguchi et al., 2015; Mochizuki et al., 2018) and in the Cascadia region of the Northeast Pacific (Heesemann et al., 2014). These observatories provide data suitable to monitor passing tsunami waves, seismic surface waves, and vertical deformation of the seafloor during earthquakes and SSEs, ultimately yielding insight into the offshore earthquake and slip processes that contribute to the characterization of earthquake and tsunami risk.

Ocean bottom pressure sensors record variations in the height of the overlying water column. After corrections are made for average water column density, which varies with changes in salinity and temperature caused by ocean circulation, seafloor pressure can capture vertical motion of the seafloor. Seafloor uplift results in a decrease in water column height above the sensor and is thus recorded as a pressure decrease, and vice-versa for seafloor subsidence (with 1 hPa equivalent to 1 cm water height). In addition to possible vertical crustal deformation signals and ocean density variations, seafloor pressure time series contain a variety of other signals at different timescales and magnitudes (Gennerich & Villinger, 2011), including ocean tides, non-tidal oceanographic variations such as currents and eddies, meteorologic effects, locality-specific disturbances due to dynamic pressure effects near canyons and other topography, sensor drift, and instrumental noise (Polster et al., 2009).

Isolating tectonic signals from the other pressure components is a principal challenge of seafloor pressure geodesy, given that pressure changes due to ocean variability can mask any centimeter-level SSE-related deformation. If the data are not processed carefully, oceanographic signals may be interpreted as tectonic deformation (Inazu et al., 2012); likewise, signals can be introduced from the processing, further masking periods of seafloor uplift. Identification of SSE-related transient deformation is particularly problematic for regions where onshore geodetic instruments lack resolution of offshore deformation processes (e.g., when they are far from the SSE source), limiting independent knowledge of SSE occurrence and timing. Accurate estimation of vertical seafloor displacement thus requires additional observations to constrain slow slip timing (such as nearby onshore GNSS displacements [Wallace et al., 2016], tremor occurrence or other seismological indicators [Araki et al., 2017], robust knowledge of oceanographic processes [e.g., Watts et al., 2021], and constraints on the direction and magnitude of sensor drift [e.g., Matsumoto & Araki, 2021; Wilcock et al., 2021]).

We present an analysis of data from a network of 14 Absolute Pressure Gauges (APGs) deployed at the Hikurangi subduction zone off the North Island of New Zealand between October 2018 and October 2019 (Barker et al., 2019; Saffer et al., 2019). Due to the known rapid instrument drift early in APG deployments (Polster et al., 2009), we use data only from January to October 2019 for this study. The APG data set spans the duration of a large SSE (March–June 2019) recorded at nearby onshore GNSS stations, which was located directly beneath the seafloor pressure sensors. Three of the sensors deployed on the central Hikurangi margin (Hawke Bay) included drift self-calibration (the A-0-A, ambient-zero-ambient, technique; e.g., Wilcock et al., 2021). Here, we demonstrate the value of self-calibrating pressure sensors to correct for sensor drift, and further show from the de-drifted data how Ocean General Circulation Models (OGCMs) can be used to identify and correct for long-period oceanographic signals that remain in the data. This study discusses the processing of the 2019 seafloor pressure sensor data and presents a set of seafloor vertical displacement estimates due to SSE activity

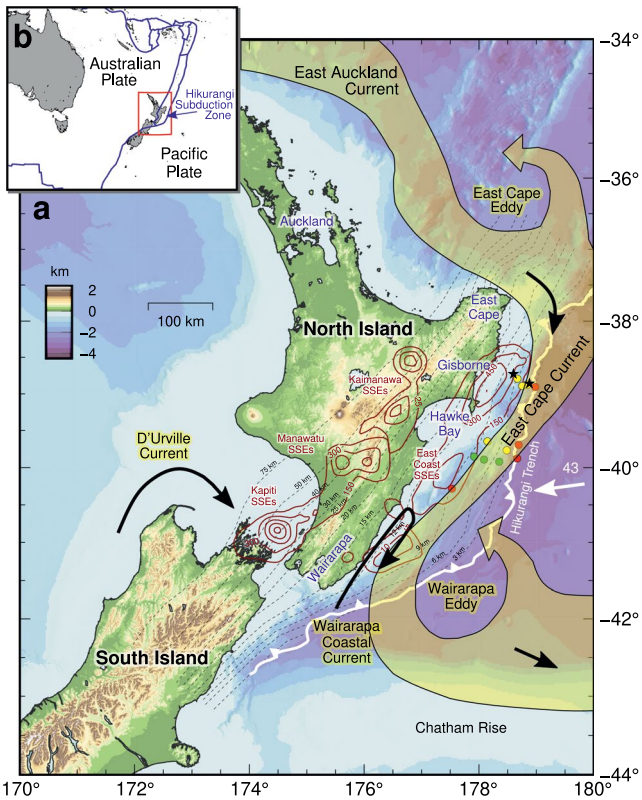

Figure 1. Tectonic and oceanographic setting at the Hikurangi Subduction Zone, North Island New Zealand. (a) Oceanographic surface currents and eddies in the proximity of the study area at the east coast of North Island are indicated by yellow shading and with black arrows (Chiswell et al., 2015). The motion (in millimeters per year) of the Pacific plate relative to the Australian plate (Beavan et al., 2002) is denoted with a white arrow and the Hikurangi Trench, the deformation front of the subduction between the Australian and Pacific plates, is shown with a solid white line east of the North Island (Barnes et al., 2010, 2018, 2020; Collot et al., 2001; Crutchley et al., 2020). The dashed gray lines are the estimated depths to the Hikurangi subduction interface (Williams et al., 2013) beneath the North Island, and the dark red contours indicate modeled slip (in millimeters) due to slow slip events (SSEs) along the Hikurangi subduction interface between 2002 and 2014 (Wallace, 2020). The seafloor instruments used in this study, from the 2019 experiment, can be seen offshore Gisborne and Hawke Bay (red, yellow and green circles; colors explained in Figure 2), in addition to offshore Gisborne IODP observatories (black stars). (b) The tectonic boundary between Australian and Pacific plates at New Zealand.

at the shallow Hikurangi subduction zone. A separate publication will be focused on resolving the spatial distribution and temporal evolution of the 2019 SSE activity, using continuous onshore GNSS data from eastern North Island, Interferometric Synthetic Aperture Radar displacements across the Gisborne region, and the seafloor vertical displacement time series we determine for the offshore Gisborne and Hawke Bay regions.

2. Tectonic and Oceanographic Setting at the Hikurangi Subduction Zone

The Hikurangi subduction zone accommodates westward subduction of the Pacific Plate beneath the North Island of New Zealand (Figure 1). The subduction of the Hikurangi Plateau, a Cretaceous Large Igneous Province on the Pacific Plate (Mortimer & Parkinson, 1996), has caused a large portion of the forearc to become subaerial. This provides a unique opportunity to investigate SSEs and earthquake processes spanning a large depth range along the plate interface (15–70 km; see dashed contours of subduction interface in Figure 1) with onshore geodetic and seismic networks. The subduction interface is estimated to lie 12–15 km below the eastern coastline of the North Island (Williams et al., 2013), and the trench (where the subduction plate interface reaches the seafloor) is located ~80–150 km offshore. While no large ($M > 7.2$) megathrust earthquakes have occurred at the Hikurangi subduction zone in the ~180 year written historical record, there is evidence from paleoseismic investigations of at least 10 possible subduction events over the past 7000 years (Clark et al., 2019; Cochran et al., 2006; Pizer et al., 2021). New Zealand's continuous GNSS network, operated by GeoNet (www.geonet.org.nz), has revealed frequent SSEs over the last two decades along the Hikurangi subduction interface (red contours in Figure 1; Wallace, 2020, and references therein). These SSEs occur at a range of depths, with diverse magnitude, duration, and recurrence characteristics, and accommodate 80%–100% of the plate motion budget within the SSE source regions at the Hikurangi subduction zone (Bartlow et al., 2014; Wallace & Beavan, 2010; Wallace et al., 2012).

SSEs along the shallow Hikurangi subduction interface (<15 km depth) have durations ranging from 1 week to 2 months and occur about every 1–2 years (Wallace, 2020). The largest of the shallow SSEs release moment equivalent to an $M \sim 7$ earthquake over several weeks and produce up to 4 cm of horizontal displacement at GNSS sites on the east coast of the North Island. The onshore geodetic observations cannot accurately resolve slip on the offshore portion of the plate boundary, leaving the deformation processes on the shallow, offshore megathrust poorly constrained. The inclusion of seafloor geodesy at subduction zones is critical to improving resolution of offshore deformation processes (Bürgmann & Chadwell, 2014), as was demonstrated by the 2014 Hikurangi Ocean Bottom Investigation of Tremor and Slow Slip (HOBITSS) experiment at the offshore northern Hikurangi subduction zone. The HOBITSS experiment used APGs to reveal centimeter-level vertical deformation of the seafloor during a large SSE in September 2014, and suggested that SSE slip extended to near the trench, to within ~2 km depth below the seafloor (Wallace et al., 2016).

Major sources of non-tidal oceanographic variations in the offshore experiment area at the Hikurangi subduction zone are the East Cape Current (ECC), the Wairarapa Coastal Current (WCC), and the Wairarapa Eddy (Figure 1; Chiswell, 2005). The ECC, assumed to extend down to 2,000 m, flows southward offshore of the northeast coast of the North Island from East Cape until it is forced eastward by the Chatham Rise. The WCC flows northward inshore of the ECC and interacts with the ECC causing variable flow at the southern and central region of the margin.

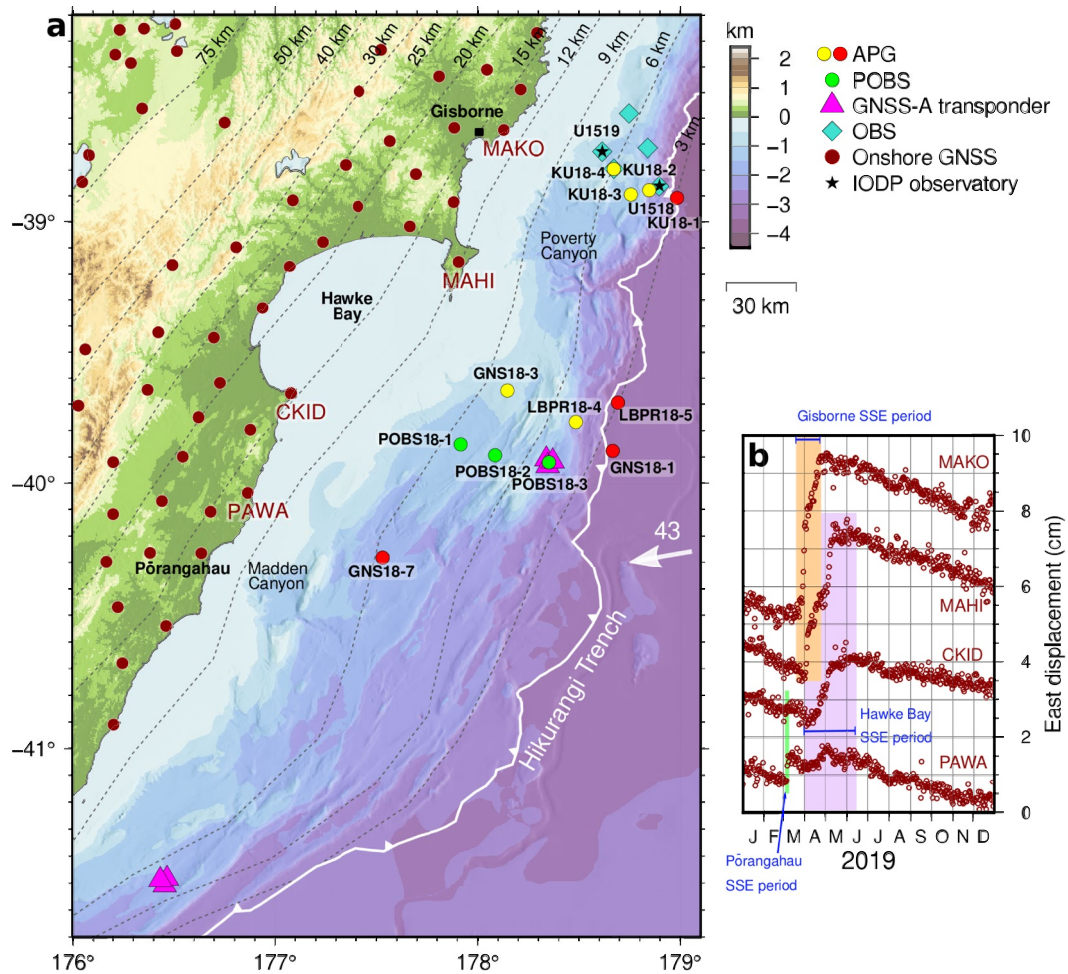

Figure 2. The locations of seafloor instruments deployed in the offshore region from the east coast of North Island, New Zealand, as part of the 2019 experiment and long-term IODP observatories. (a) The offshore sensors used in this study are the APGs (yellow circles; with reference sites in red), POBSs (green circles), and seafloor pressure data from the IODP observatories (black stars). Other types of instrumentation from the 2019 experiment, such as GNSS-Acoustic arrays (magenta triangles) and ocean bottom seismometers (OBS; turquoise diamonds), are also shown. The GeoNet onshore GNSS network is indicated with dark red circles, and the Hikurangi trench (solid white line) and Hikurangi subduction interface depth contours (dashed gray lines) are also shown. (b) East displacement in centimeters of four continuous GNSS time series (MAKO, MAHI, CKID, and PAWA) from 1 January 2019 to 31 December 2019, with slow slip periods highlighted with orange shading for offshore Gisborne SSEs, lavender shading for Hawke Bay SSEs, and green shading for Pōrangahau SSEs.

3. Pressure Data Processing Techniques

3.1. Instrumentation

In this paper we resolve SSE-related vertical deformation from seafloor pressure sensors at the Hikurangi subduction zone in 2019 (Figure 2), during a collaborative deployment involving instruments and scientists from New Zealand, Japan, and the United States. The experiment deployed 19 APGs, five short-period Ocean Bottom Seismometers (OBS), and three Pressure-Ocean Bottom Seismometers (POBS; pressure sensors equipped with A-0-A drift correction - described in Section 3.3) off the east coast of North Island, New Zealand, from October 2018 to November 2019 (Barker et al., 2019). In addition to these, we include seafloor pressure time series from the wellhead at two subseafloor International Ocean Discovery Program (IODP) observatories installed offshore of the Gisborne region in 2018 (Saffer et al., 2019).

A large SSE occurred beneath the seafloor array from March 2019 to June 2019. Figure 2 shows the locations of the pressure sensors from the 2019 seafloor deployment relative to the onshore GNSS sites, and the timing of slow slip indicated by the eastward motion of GNSS sites MAKO, MAHI, CKID, and PAWA. Ten of the 24

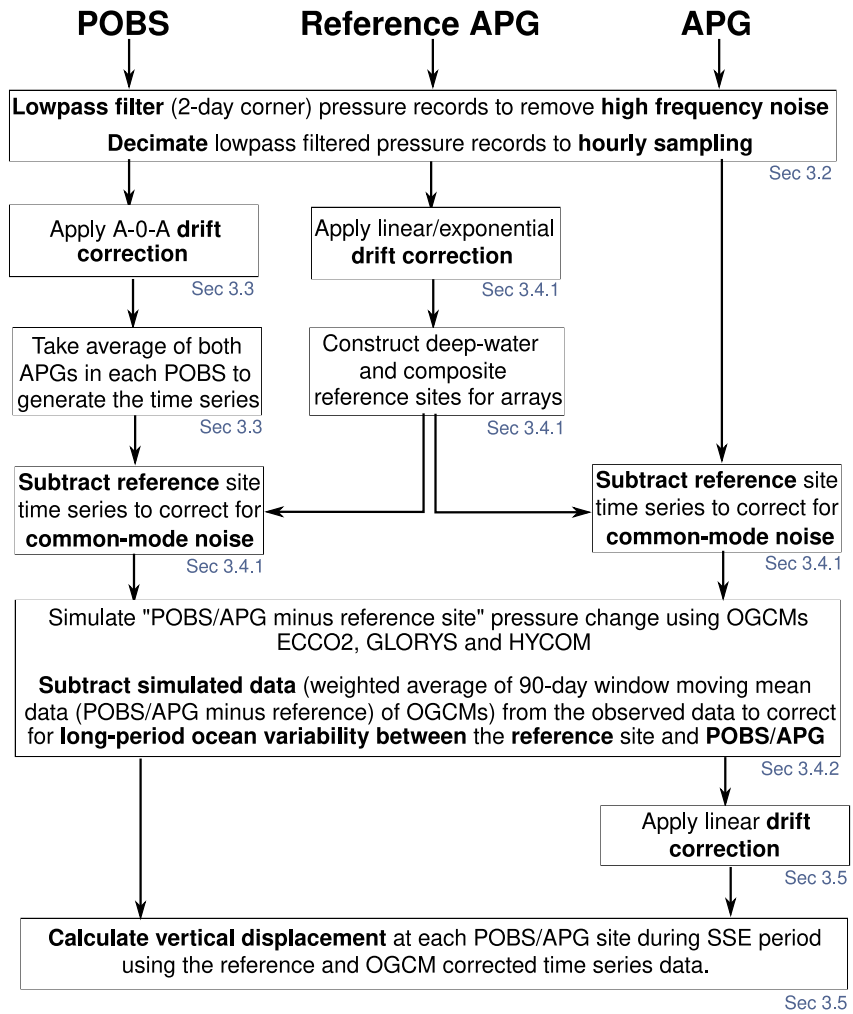

Figure 3. Processing sequence for the pressure data in this study. The data types are separated into POBS, reference APG, and APG (i.e., main array APGs without self-calibration) to highlight the specific processing required by each type. The section where the detailed description of the processing can be found is indicated beneath each step.

pressure sensors deployed had problems, so in total we analyze pressure records from 11 APG and three POBS sites (see Table S1 in Supporting Information S1 for pressure sensor deployment details).

3.2. Processing Sequence

To resolve any vertical tectonic signals in the seafloor pressure data recorded during our 2019 experiment, we focus on correcting for the sensor drift and oceanographic components. We use all pressure data beginning from 1 January 2019, which excludes the first three months of data (in late 2018) to avoid initial nonlinear and more rapid sensor drift typical of APGs (Polster et al., 2009) for the sensors that are not equipped with self-calibration (A-0-A). The processing sequence for the pressure data in this study is outlined in Figure 3. Tides (diurnal and semi-diurnal) and other high frequency noise are removed using a 2-day corner lowpass filter, and the filtered data are then decimated to hourly sampling. The remaining sequence of processing steps involves correcting for drift of the POBS sensor data (carried out prior to the full processing of all instruments in the deployment, detailed in Section 3.3), correcting for non-tidal oceanographic processes (using reference pressure sites outside the SSE region, in combination with OGCMs, detailed in Section 3.4), and removal of linear sensor drift for the main array APGs without A-0-A (Section 3.5).

3.3. Drift Correction of Self-Calibrating Pressure Sensors

The drift of pressure sensors after deployment is typically characterized as an initial rapid drift which exponentially decays with time (Polster et al., 2009). The drift is unique to each sensor, and even after the rapid, early drift phase can reach amplitudes equivalent to several tens of centimeters of water depth per year. Techniques to remove sensor drift include fitting and subtracting exponential and linear functions (Muramoto et al., 2019) or polynomials (Fredrickson et al., 2019; Wallace et al., 2016), using pre-deployment laboratory tests and in situ observations to assess sensor specific drift characteristics (Matsumoto & Araki, 2021), and more recently, by deploying self-calibrating pressure sensors (Wilcock et al., 2021).

The three POBS sensors deployed during the 2019 experiment were each composed of a three-component accelerometer and two A-0-A equipped pressure gauges (referred to as APG1 and APG2 for each POBS in Figure 4). We do not use the accelerometer data from the POBS instruments in this study, and from hereafter use "POBS" to refer to the drift-corrected pressures sensors. To implement A-0-A, the pressure gauge's valve closes to the seawater pressure ("A") every 7 days and opens to the internal pressure of the sensor housing ("0"), which is also independently measured using a barometer. The valve then opens back to seawater pressure ("A") 5 min later. The sensor drift of each gauge is calculated by comparing the internal casing pressure measured during the switch periods ("0") to the stable barometer's pressure reading. Assuming the APG drift at low pressure (inside the housing) is the same at high pressure (e.g., when the valve opens to seafloor pressure), the respective calculated drift trends (Figure 4b) can be subtracted from the seafloor APG data for each POBS (Figure 4c)—an assumption previously inspected by laboratory tests switching between piston gauge and atmospheric calibrations (Sasagawa et al., 2018). Prior to this 2019 experiment, the POBS sensors had been successfully tested for two weeks offshore of Long Island, NY, but this was the first deployment of the POBS sensors on the seafloor with the aim of capturing vertical seafloor deformation.

Prior to the A-0-A correction, the gauges all show linear trends of decreasing pressure (following the initial rapid drift phase) ranging from 8.9 to 67.6 hPa/yr (Figure 4). The apparent drift for these POBS instruments is higher than typical for these pressure sensors (Polster et al., 2009) because a component of the drift is related to loss of voltage regulation for the pressure sensors. This was caused by battery voltages falling too low later in the deployment to provide an adequate overhead for the voltage regulators in the pressure sensors. Fortunately, the A-0-A method removes this source of drift as well as normal sensor drift. The residual linear trend is reduced to −0.1–5.6 hPa/yr after applying A-0-A calibration to each pressure gauge (which drift at different rates). In the case of all three POBS sensors, the residual linear trend of the two gauges within the same POBS is brought to within 0.7–2.5 hPa/yr of each other (equivalent to a difference in pressure variation of ∼0.06–0.2 hPa over 1 month). The significant reduction of the linear trend clearly demonstrates minimization of sensor drift by the A-0-A method, with the A-0-A method capable of correcting even the non-linear component of sensor drift to an estimated accuracy of a couple of centimeters per year (see Figure 4c). After the A-0-A drift correction, the average pressure value from the two gauges is used for the POBS instrument pressure time series in the remainder of this study.

3.4. Ocean Noise Analysis and Correction

Ocean noise recorded by seafloor pressure sensors is due to regional and global ocean circulation effects, including currents and eddies (e.g., the ECC, WCC, and the Wairarapa Eddy at the Hikurangi subduction zone in Figure 1, Chiswell, 2005), and ocean tides which are easily removed with low-pass filtering. Noise related to ocean circulation is larger at shallower water locations (for example, 900 vs. 1,900 m), varies seasonally, and is influenced by site-specific seafloor topography and proximity to coastlines. Weather-related pressure variations are largely compensated by deformation of the sea surface. Removal of oceanographic noise from APG time series for seafloor geodetic studies is typically done by either (a) using a reference APG deployed in close proximity, assuming that the oceanographic noise is common-mode across the network (Davis et al., 2015; Ito et al., 2013; Wallace et al., 2016), or (b) using simulated seafloor pressure data from OGCMs (Dobashi & Inazu, 2021; Gomberg et al., 2019; Muramoto et al., 2019). Thus far, the reference station method has produced the best results in terms of APG data variance reduction (e.g., Fredrickson et al., 2019; Inoue et al., 2021; Muramoto et al., 2019).

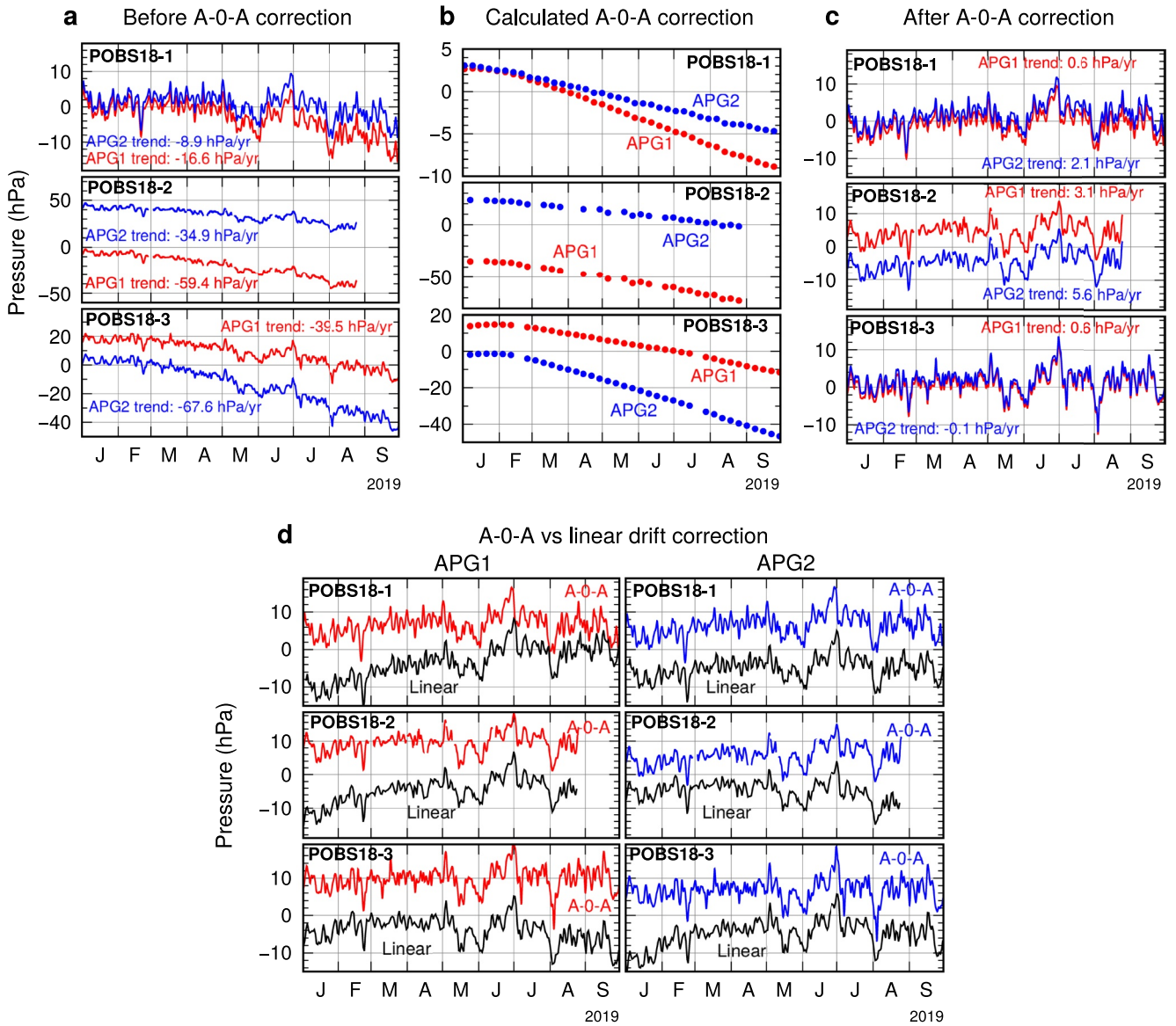

Figure 4. The A-0-A drift correction of the three self-calibrating pressure sensors, POBS18-1, POBS18-2, and POBS18-3, in the 2019 Hikurangi experiment. (a) The raw lowpass filtered observations of the two pressure gauges (APG1—red, APG2—blue) on each instrument prior to A-0-A drift correction. (b) The instrument drift of the two gauges calculated using 7-day A-0-A (internal casing) measurements. (c) The two gauges of each instrument after the A-0-A drift correction has been applied (i.e., time series in subplot a minus A-0-A correction in subplot [b]). (d) Comparison of applying linear drift correction of the POBS data following the traditional drift correction method (black) versus drift correction using the A-0-A measurements (red and blue for APG1 and APG2 respectively). Residual linear trends, displayed in subplots (a and c), calculated for the 2019 period used in this study are indicated in hectopascals per year. For all subplots, the time series have been adjusted to plot close to zero, however the difference between the two gauges (both raw and corrected) has been preserved for subplots (a–c). Pressure is shown in hectopascals (hPa); an increase in pressure is equivalent to an increase in the height of the water column.

3.4.1. Locally Deployed Reference Sites to Reduce Common-Mode Noise

To correct for ocean noise in the APG data, we deployed reference APGs away from the region expected to undergo tectonic deformation. Subtracting the reference site data from the pressure data overlying the SSE source reduces the level of ocean noise, assuming the oceanographic signal is common-mode through the region. Two types of reference sites are tested for common-mode noise reduction: (a) deep-water reference sites located on the subducting plate, east of the Hikurangi Trench (KU18-1, GNS18-1, and LBPR18-5 in Figures 2) and (b) a reference site located along-strike from the deformation region (GNS18-7), at a similar water depth to the array of sensors overlying the SSE region. The former approach has been used previously at the Hikurangi subduction zone (Wallace et al., 2016), whereas the latter follows a recently proposed optimal configuration of pressure

sensors at water depths similar to the sites overlying the SSE region, but outside the SSE region (Fredrickson et al., 2019). Fredrickson et al. (2019) demonstrated a clear depth-dependence of oceanographic variations in APG data from Cascadia, and such depth dependence was also observed in the 2014 HOBITSS experiment in the northern portion of our study area (Inoue et al., 2021).

Before the reference site data are subtracted from the pressure data of sites overlying the SSE deformation region (to reduce the level of ocean noise), the reference sites are corrected for instrument drift. It is important to note that non-reference APGs without A-0-A self-calibration are drift corrected after applying ocean noise corrections rather than at this stage (see processing sequence in Figure 3), as the reduced data noise levels later in the processing sequence allow for a more accurate estimation and correction of the drift. The earlier drift correction of the reference sites is required because our investigation involves combining multiple APGs (which drift at different rates and directions) to construct our deep-water and composite reference sites. To remove instrumental drift, most of the 2019 reference site pressure time series are fitted with a linear function, which is subsequently subtracted to correct for drift (Figure S1 in Supporting Information S1). This assumes that after the first couple of months of the deployment, the early rapid drift of these sensors has decayed to a linear trend (following the drift correction methodology of previous studies; e.g., Wallace et al., 2016). The drift of reference APG GNS18-1 shows a significant exponential component in decay even after the first couple of months of the deployment, so a two-term exponential function is required for de-drifting.

The GNS18-7 sensor, located along-strike from the arrays at 1,895 m water depth, is more suitable to use as a reference site because it is in similar water depths to the rest of the array (779–2,207 m deep), compared to the deep-water reference sites. Onshore GNSS instrumentation adjacent to GNS18-7 (e.g., PAWA in Figure 2) suggest that the use of GNS18-7 as a reference site is appropriate, as no substantial slow slip events were observed at PAWA that could impact the GNS18-7 pressure time series. A rapid period of offshore slow slip occurred in early March, prior to the deployment of GNS18-7. After the deployment of GNS18-7, ∼0.5 cm of eastward motion is observed at PAWA; however, PAWA is at the southern edge of the main 2019 SSE activity detected more clearly on northern stations such as CKID, thus indicating that GNS18-7 is unlikely to be impacted by vertical deformation.

Due to a later deployment of GNS18-7 (in March 2019), composite reference sites (using GNS18-7 and a deep water reference site for prior to March 2019) are created to act as the similar water depth reference site for the Gisborne and Hawke Bay arrays. To construct the composite reference site, the offset between the time series (between the respective deep-water reference site and GNS18-7) is estimated by averaging the 25 March 2019 data and merging the two time series together, leaving pre-25 March data as the deep reference time series and post-25 March data as the GNS18-7 time series.

3.4.1.1. Hawke Bay Reference Site Data

For the Hawke Bay deep-water reference APG time series, the average of LBPR18-5 and GNS18-1 is used (Figure 2 and Figure S2 in Supporting Information S1). The Hawke Bay composite reference site consists of the deep-water reference site (average of LBPR18-5 and GNS18-1) from 1 January 2019 to 25 March 2019 and GNS18-7 (25 March 2019 onwards), as explained above. The pressure sensors overlying the Hawke Bay SSE region have depths ranging from 779 to 2,207 m, with the composite reference site at 1,895 m depth (GNS18-7), and the deep-water reference sites at depths of 3,309 and 3,311 m (GNS18-1 and LBPR18-5).

The ocean noise correction using the composite reference site results in a lower root-mean-square (RMS) value for the POBS sensors in the Hawke Bay area, compared to corrections using the deep-water reference site (January to October black and gray bars in Figure 5), whereas LBPR18-4 and GNS18-3 have increased RMS values. After subtracting the deep-water reference site from the APG data, we note a transition in seafloor pressure variations from July 2019 at all Hawke Bay sites (Figures 6d–6f and Figures S3–S7 in Supporting Information S1). During this July–October austral winter/spring period, larger amplitude pressure variations (up to 8 cm) occur over 1–2-month periods, whereas this is not observed after subtracting the shallower reference site or during summer/autumn (January–June). Separate RMS analysis of the January–June and July–October periods (Figure 5) reveals that the composite reference site most effectively reduces ocean noise for all sites and periods, except for pressure variations between January and June at GNS18-3. That this correction is better is unsurprising given the depth-dependence of APG signals (due to similarities in ocean variability along bathymetric contours) observed by Fredrickson et al. (2019) and Inoue et al. (2021). The APGs/POBSs are closer in depth

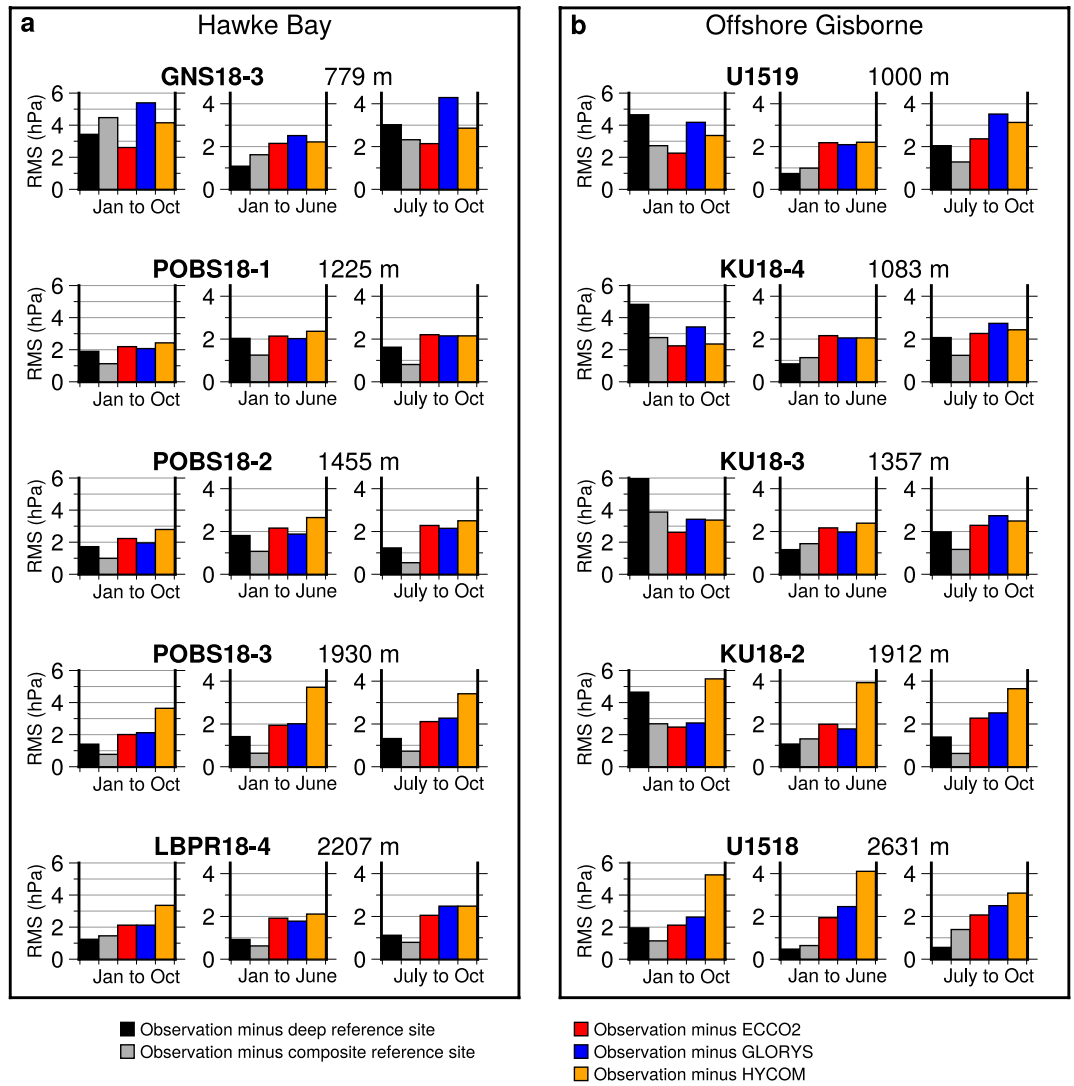

Figure 5. Root-mean-square (RMS in hPa) values of the time series for pressure sensors overlying the SSE regions, after ocean noise correction using the deep-water reference site (black), composite reference site (gray), and simulations of pressure at each site from Ocean General Circulation Models: ECCO2 (red), GLORYS (blue), and HYCOM (orange). For (a) the Hawke Bay array and (b) the offshore Gisborne array, three sets of RMS values are presented: January–October (the whole data period), January–June (the period containing the SSE), and July–October (the period after the SSE). The long-period ocean variability correction described in Section 3.4.2 is not included in the processing for the data analyzed in these RMS charts.

to the composite reference site than the deep-water reference site, therefore the reduction in noise level is likely due to the composite reference site recording more similar pressure variations on the slope caused by eddies and currents. As a result, we proceed to process the Hawke Bay data using the de-drifted time series of the composite reference site for the common-mode ocean noise corrections.

3.4.1.2. Offshore Gisborne Reference Site Data

For the APG array offshore Gisborne, KU18-1 is used as the deep-water reference site and the composite reference site is created using KU18-1 (1 January–25 March) and GNS18-7 (25 March onwards) time series data (Figure S2 in Supporting Information S1). The pressure sensors overlying the Gisborne SSE region range from 1,000 m depth to 2,631 m, with the shallow- and deep-water reference sites located at 1,895 m (GNS18-7) and 3,483 m (KU18-1), respectively.

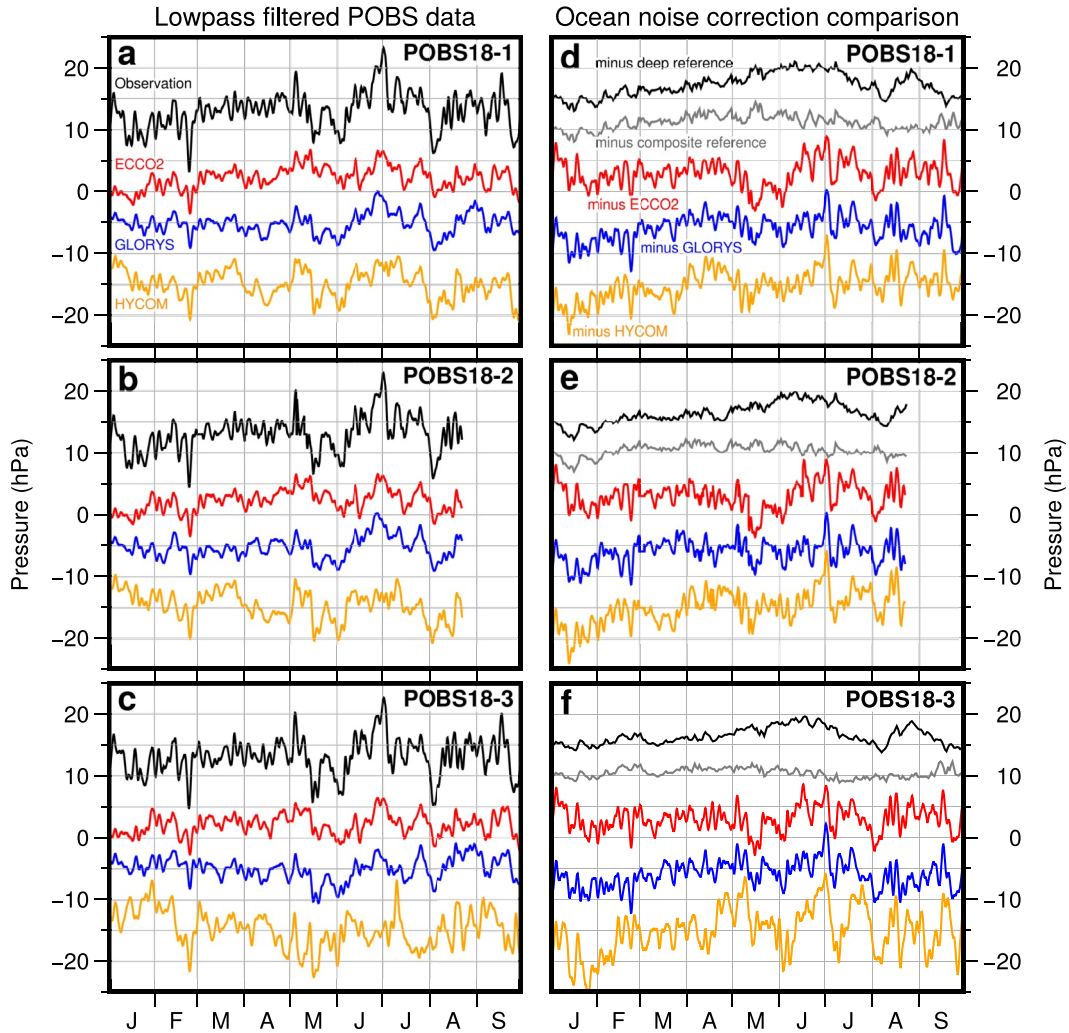

Figure 6. Two-day corner lowpass filtered observed pressure data (black) for each self-calibrating POBS sensor (a–c) in the deployment compared to the simulated data from the ECCO2 (red), GLORYS (blue), and HYCOM (orange) OGCMs. The ocean noise correction of each POBS sensor after subtracting either the OGCM simulation or reference site is also shown using the same colors for the OGCMs, black for the deep reference site, and gray for the composite reference site (d–f). All subplots present pressure with the convention that an increase in the height of the water column is shown as a positive pressure change.

Analysis of the Gisborne array entire time series RMS values suggests that the deep-water reference site is significantly worse at reducing ocean noise compared to the composite reference site (January to October bar plots in Figure 5). However, after analyzing the January–June and July–October periods separately, it is clear the large RMS values for the deep-water reference site data result from the same shift to larger winter/spring pressure fluctuations observed after July 2019 at the Hawke Bay array (Figures S8–S12 in Supporting Information S1). Despite there being a convincing reduction in the overall noise level for the Gisborne APGs after subtracting the composite reference site, this impact is limited to the pressure variations recorded from July 2019 onwards, outside our period of interest (April–May 2019, see MAKO SSE period in Figure 2).

Neither the deep-water nor composite reference site is significantly more effective at reducing January–June noise levels across the sites in the Gisborne array, so we have chosen the deep-water reference site for common-mode noise reduction because of its proximity (i.e., tens of km to the Gisborne array vs. ∼180 km from the composite site to the array). There are complex bathymetric features, such as Poverty Canyon (Figure 2), lying between the GNS18-7 and the Gisborne APG array, which may influence the ocean circulation in the region, resulting in sub-regional differences in oceanographic signals. More variability in mesoscale signals recorded by the

composite reference site and Gisborne APGs may arise from the interaction of the Wairarapa Coastal Current with the East Cape Current at the southern Hikurangi subduction zone (Chiswell et al., 2015). The interaction of currents could cause variable flow which will be recorded by GNS18-7 and possibly the Hawke Bay array, but the Gisborne array is likely too far north for the same signals to be present (located ∼180 km along-strike from GNS18-7). The closer APGs/POBSs overlying the Hawke Bay SSE deformation region are not suitable to use as a similar water depth reference site as they may contain SSE-related pressure changes. Therefore, to correct for common-mode ocean noise at the Gisborne array, we subtract the data recorded by the de-drifted time series of the deep-water reference site.

3.4.2. Ocean General Circulation Models (OGCMs) Used to Characterize Long-Period Oceanographic Variations

Another approach to assessing the contribution of ocean noise in seafloor pressure data draws on simulations of global or regional ocean circulation. While OGCMs have been found not to be accurate enough to directly correct APG observations (for tectonic studies requiring centimeter-level resolution, or ∼1 hPa), they are able to simulate changes to the overlying water column in a generalized way (Dobashi & Inazu, 2021; Fredrickson et al., 2019; Gomberg et al., 2019; Inazu et al., 2012; Muramoto et al., 2019; Wilcock et al., 2021). Three global, baroclinic OGCMs are incorporated into our pressure data processing: ECCO2 (Estimating the Circulation and Climate of the Ocean project; Menemenlis et al., 2008), GLORYS (GLobal Ocean ReanalYsis and Simulation; Lellouche et al., 2021), and HYCOM (HYbrid Coordinate Ocean Model; Cummings, 2006; Cummings & Smedstad, 2013; Helber et al., 2013). Table 1 provides an overview of the three OGCMs, and Text S1–S3 in Supporting Information S1 contains further details on the extraction and formatting of the OGCM seafloor pressure data.

Table 1
HYCOM, GLORYS, and ECCO2 OGCM Details

	HYCOM	GLORYS	ECCO2
Base model	HYCOM	NEMO v3.1	MITgem
Horizontal resolution	1/12° between 40°S and 40°N	1/12°	1/4°
	1/24° poleward of 40°N/S		
Vertical levels	41 hybrid levels	50 *z*-coordinate levels	50 z-coordinates (ranging in thickness from 10 m near surface to ∼250 m)
Atmospheric forcing	NAVGEM 2.0	ERA-Interim	NCEP
		ERA5 starting in 2019	
Assimilated observations	Satellite altimetry	Delayed Time SLA (all satellites)	Satellite altimetry
	Satellite and in situ SST	Reynolds 1/4° AVHRR SST	GRACE ocean bottom pressure
	In situ T/S profiles from XBTs, Argo floats, moored buoys	In situ T/S profiles from CORAv4.1[a]	AVHRR SST
			Aquarius SSS
			In situ T/S profiles from Argo, CTD, XBT
			ITP, APB, Gliders
			TAO mooring
			Global mean SSH and OBP
Bathymetry	GEBCO 30 arc-second	ETOPO1 for deep ocean	Combination of Smith and Sandwell (1997) and GEBCO 1 arc-minute
		GEBCO 30 arc-second for coast and continental shelf[b]	

Note. APB, autonomous pinniped bathythermograph; AVHRR, advanced very high resolution radiometer; CTD, conductivity, temperature, and depth; ERA, ECMWF Re-Analysis; ECMWF, European Centre for Medium-Range Weather Forecasts; GEBCO, General Bathymetric Chart of the Oceans; GRACE, Gravity Recovery and Climate Experiment; ITP, ice-tethered profiler; MITgem, MIT General Circulation Model; NAVGEM, Navy Global Environmental Model; NEMO, Nucleus for European Modeling of the Ocean, OBP, ocean bottom pressure; SLA, sea-level anomalies; SSS, sea-surface salinity; SST, sea-surface temperature; T/S, temperature—salinity; TAO, Tropical Atmosphere Ocean; XBT, expendable bathythermograph.

[a]CORA (Coriolis Ocean Data Set for Reanalysis) integrates data from autonomous platforms (Argo, fixed moorings, gliders, drifters, sea mammals), and research or opportunity vessels (CTDs, XBTs, ferrybox). [b]ETOPO1 is used in regions >300 m and GEBCO in regions <200 m with a linear interpolation in the 200–300 m range.

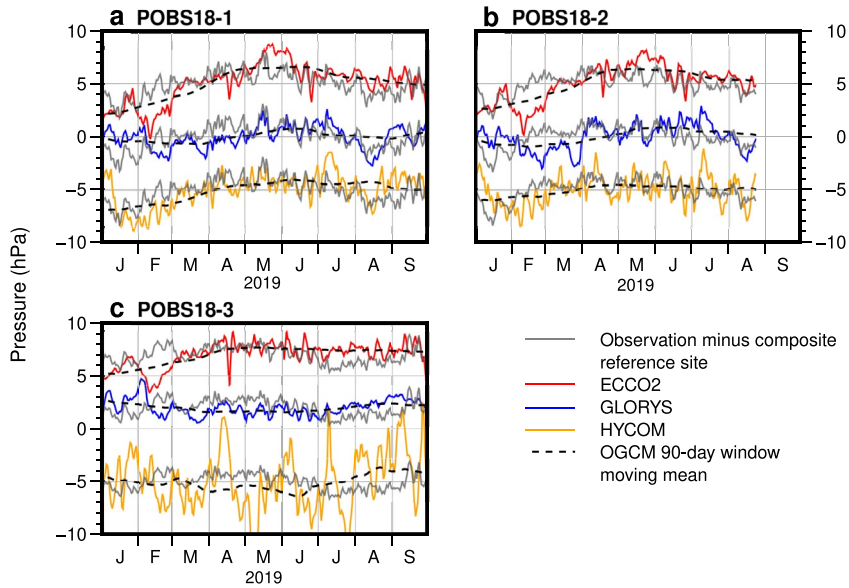

Figure 7. The recorded data (gray) of the three self-calibrating POBS sensors after A-0-A correction and subtraction of the Hawke Bay composite reference site. The simulated difference between the POBS and reference site using the OGCMs are overlain for comparison. Pressure is shown with the convention that an increase in the height of the water column is shown as a positive pressure change. The time series have been offset for visualization purposes; however, there has been no alteration to the amplitudes of the data.

Similar to previous studies (Muramoto et al., 2019; Wallace et al., 2016), we find that the reference sites are more effective in reducing oceanographic noise levels than the OGCMs when applied as a direct correction. This is demonstrated by the comparatively lower reference site-corrected RMS values during our period of interest (January–July bars in Figure 5), the clearly quieter reference site-corrected time series (Figures 6d–6f) relative to the OGCM-corrected data, and an observable power reduction across most periods when subtracting the reference site data but not when subtracting the OGCMs (Figures S13–S15 in Supporting Information S1). Therefore, the reference site method is applied to reduce common-mode noise, rather than directly subtracting the seafloor pressure variations simulated at each main array site by the OGCMs. Dobashi and Inazu (2021) showed that the inclusion of atmospheric pressure to OGCMs, which is not considered in our study, resulted in an RMS reduction of ∼15% at the Hikurangi Trough. On the other hand, Androsov et al. (2020) found only a modest correlation between simulated seafloor pressure and observed seafloor pressure in a region of high eddy activity and frontal meandering, even when atmospheric pressure was included. Incorporating atmospheric pressure to the OGCM results presented here is beyond the scope of the present study. However, based on the results of Dobashi and Inazu (2021) the current estimates (Figures 5 and 6) could be improved by as much as 15% by incorporating atmospheric pressure.

After investigating the difference in ocean variability between each POBS sensor and the reference site using only the OGCMs, we see some similarity in long-term trends (several months) between the modeled and recorded data (Figure 7). This indicates that long term trends due to ocean noise, which vary over the length scales of the APG spacing, likely remain in the observed data after the correction using a locally deployed reference site, and thus could influence the inferred vertical displacement. We estimate long term oceanographic variations between the seafloor pressure sites and the reference sites using the three OGCMs (black dashes in Figure 7 and Figures S3–S12 in Supporting Information S1), which we then remove from the observed data. The long-period variations are calculated by taking a 90-day window moving mean of the OGCM pressure data. To apply a single correction for each observed "APG minus reference" pair in the experiment, we take a weighted average of the three OGCM long term pressure variations for each pair, with weighting of the OGCMs informed by the cross-correlation coefficient of the observed data with the OGCM data for the APG-reference pair. The details of this calculation and our reasoning behind these choices can be found in Text S4 of Supporting Information S1. The weighted average of the 90-day window moving means of the OGCM pressure data is then subtracted from the respective reference-site-corrected observed pressure data as a long-period ocean variability correction.

3.5. Drift Correction

Following the corrections for ocean noise, we estimate the sensor drift based on the pressure data (for APG sites not equipped with self-calibration) by excluding the time period of the 2019 SSE, thus avoiding incorporating potential SSE displacement into the drift estimate (which could mask the SSE). The SSE timing is constrained by east component onshore GNSS data from CKID for the Hawke Bay array and MAKO for the offshore Gisborne array. The Hawke Bay sensors (GNS18-3 and LBPR18-4) are drift corrected using data from 1 January to 1 April—the 3 months prior to onset of slow slip at CKID. Data after the termination of SSE-related motion at CKID are not used in the estimation of drift, due to the potential for delayed offshore deformation suggested by the self-calibrated POBS data.

For the offshore Gisborne sensors, the data from the 1 January–15 March and 25 April–1 July periods are used to estimate drift. Gisborne data from July to October are excluded from the estimation of drift due to large amplitude signals that we think are ocean noise. We justify this as an impact of winter abruptly raising the effective noise level but acknowledge the limitations of our data in resolving oceanographic noise effects throughout the time series. If due to tectonic deformation, we would expect significant displacement to be observed onshore (at MAKO; larger amplitude than the March-May displacements), which is not detected. Figures S8–S12 in Supporting Information S1 show OGCMs GLORYS and HYCOM predict similar pressure variations, suggesting the signals are of oceanographic origin. Using a least squares approach, a linear function is fit to the selected periods of the ocean noise corrected time series, with offsets for masked (SSE) periods bounded by data for the Gisborne sensors (e.g., Figure S16 in Supporting Information S1). The calculated linear trend is subtracted from the respective differenced data to correct for the remaining sensor drift (see Figure 8 for fully processed time series data). We then estimate the vertical displacement for each site by calculating the means of the drift-corrected data from before and after the slow slip periods (indicated by blue horizontal lines in Figure 8). The vertical displacement uncertainties are determined using the RMS values of the data involved in the displacement calculation.

4. Results

4.1. Hawke Bay Vertical Displacement

In the offshore Hawke's Bay area, SSE onset is detected at the Cape Kidnappers GNSS site (CKID) in the first week of April and the motion ends in early June (Figure 8). After full processing of the seafloor pressure sensor data, a gradual pressure decrease is visible at POBS18-1 and POBS18-2 from early April to June/July, which we interpret as uplift of the seafloor (black data in Figure 8). In Figure 9 we display the estimated vertical displacements in map view, with and without the long-period ocean variability correction, showing that this correction results in an increase in displacement estimates at POBS18-1 (from -0.3 ± 0.9 cm to 1.4 ± 0.8 cm), POBS18-2 (from -0.1 ± 0.8 cm to 1.1 ± 0.7 cm), and POBS18-3 (from 0.8 ± 0.5 cm to 1.7 ± 0.5 cm). GNS18-3 is the shallowest of the Hawke Bay array and appears to experience the largest uplift in this region. This is also the site with the largest impact of the long-period ocean variability correction, however, the displacement estimate is reduced by 2.6 cm, from 5.3 ± 1.4 cm to 2.7 ± 1.1 cm. Timing of the offset at GNS18-3, if due to SSE-related uplift, is challenging to determine due to large fluctuations (as much as 5 cm) from May to August, suggesting that the ocean noise may not be fully removed at this site.

The POBS18-3 time series shows no obvious pressure change throughout April and May, but a pressure decrease (e.g., equivalent to uplift) is observed during June. This signal is delayed relative to the timing from onshore GNSS (Figure 8). POBS18-3 is the closest POBS sensor to the Hikurangi trench; therefore, delayed uplift could be an indication of prolonged slow slip beneath Hawke Bay, involving a relatively narrow SSE slip patch that has migrated updip. A similar delayed uplift signal (equivalent to 2.0 ± 0.4 cm) is also observed at LBPR18-4 (22.5 km to the north of POBS18-3). POBS18-3 and LBPR18-4 are located well beyond where slip can be resolved with onshore geodetic instrumentation; so the onshore GNSS network cannot be used to confirm the persistence of the SSE near the trench through June. None of the OGCMs, apart from GLORYS for LBPR18-4, predict a decrease in pressure during June (Figure S7 in Supporting Information S1), suggesting that the observed pressure decrease may indeed be tectonic in origin. GLORYS simulates a pressure decrease with similar amplitude to the observed signal at LBPR18-4 during June; however, the predicted decrease continues throughout July and August, deviating significantly from the observations. In general, the GLORYS simulation for this site is noisy and often appears inaccurate and provides equivocal evidence that the observed delayed offset may be

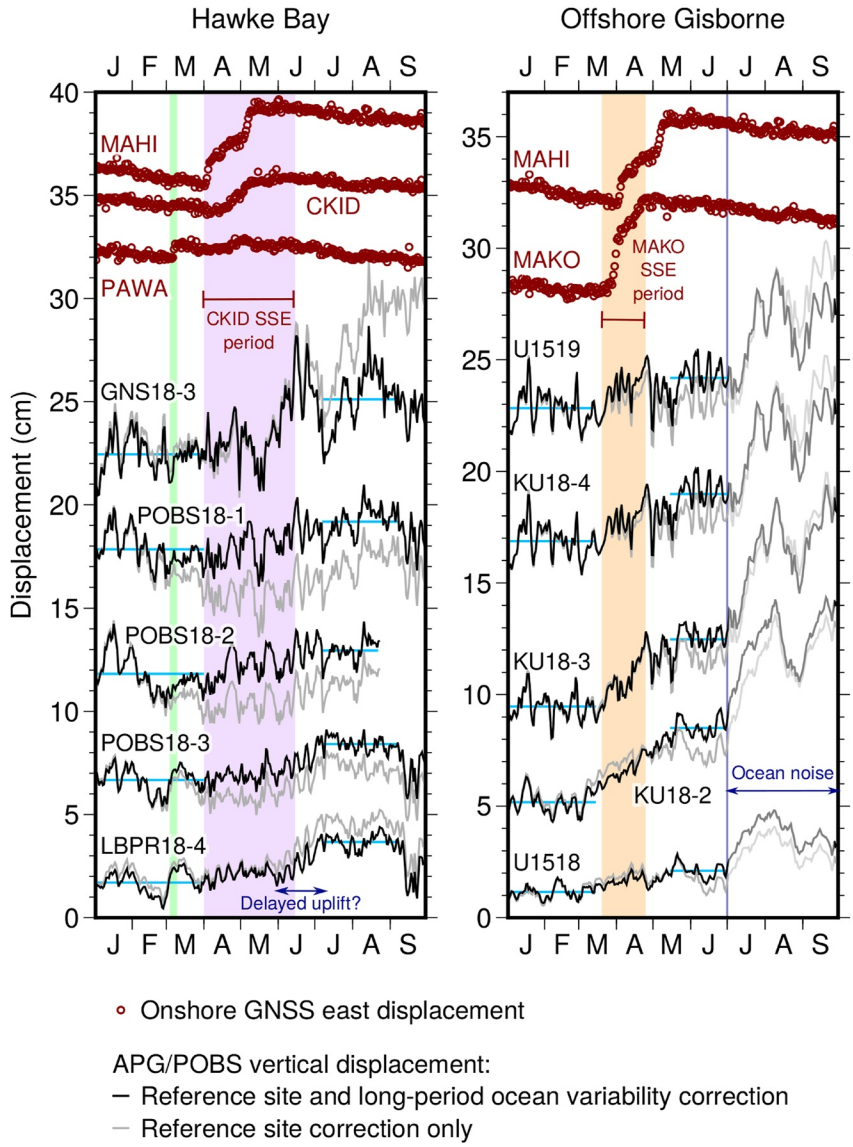

Figure 8. The equivalent vertical displacement of seafloor pressure sensors after ocean noise and drift correction, in centimeters. This involves having applied an ocean noise correction using only reference sites (gray), or reference sites and an additional 90-day window moving mean of OGCM simulations for long-period ocean variability (black). The horizontal blue lines denote the period used to calculate the vertical displacement estimates. Green and lavender shading indicates periods of slow slip from the onshore PAWA and CKID GNSS stations respectively for the Hawke Bay array, and orange shading indicates the MAKO SSE period for the Gisborne array. The PAWA, CKID, MAHI, and MAKO east component data, in centimeters, are shown as dark red outlined circles at the top of each time series subplot. Offshore Gisborne pressure data from July to October is faded relative to the rest of the time series as we think the large amplitude signals are ocean noise. Pressure data are presented in centimeters with the convention that uplift of the seafloor is indicated as an increase in displacement. The time series have been offset for visualization purposes; however, there has been no alteration to the amplitudes of the data.

wholly oceanographic. If all the OGCMs contained the same signal, then there would be a stronger argument for the delayed pressure decrease signal being of oceanographic origin. Thus, we suggest that the seafloor pressure decreases reflect updip migration of 2019 slow slip along the subduction interface east of Hawke Bay, although further investigations, such as future deployments of denser seafloor arrays in this area, are needed to verify this behavior.

A rapid decrease in pressure (possible uplift) at POBS18-3 and LBPR18-4 is observed at the end of February (Figure 8), which occurs 6 days before SSE-related eastward motion of GNSS site PAWA, located ~130 km from

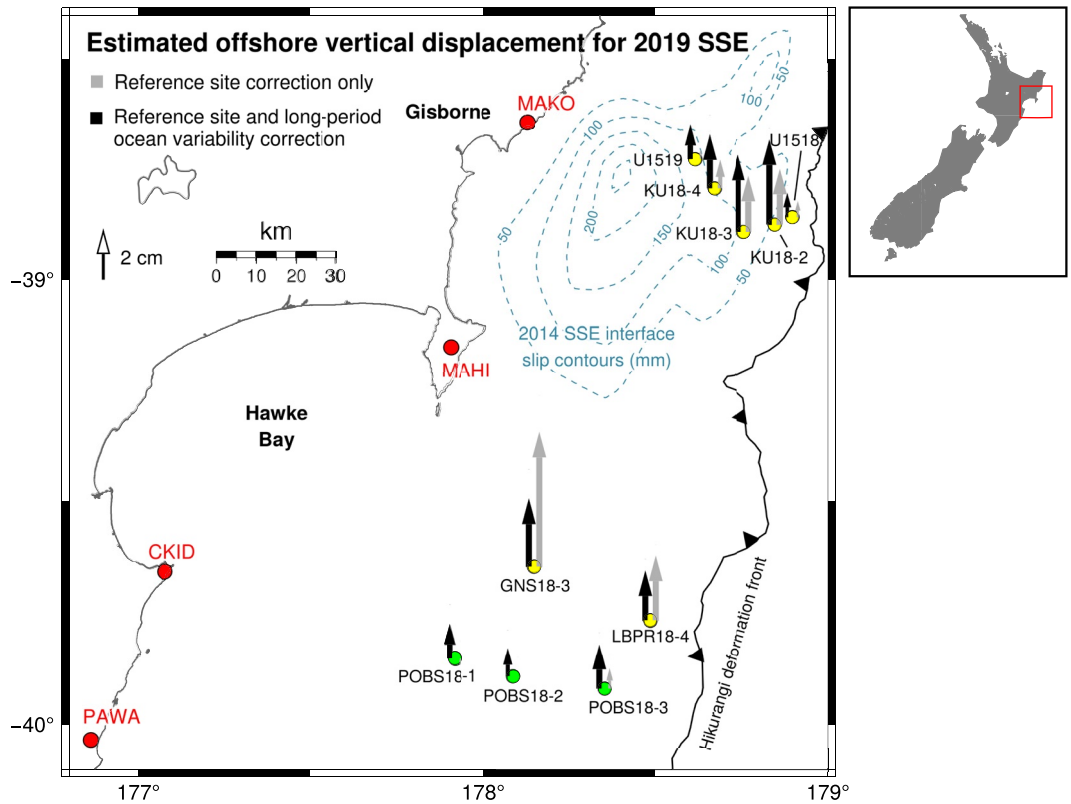

Figure 9. Estimated offshore vertical displacements for the 2019 SSE. Displacements are calculated using the equivalent vertical displacement time series of seafloor pressure sensors (APGs and POBSs; yellow and green circles respectively) after ocean noise and drift correction. The gray data involve ocean noise correction using only a reference site, and the black data (the preferred data) involve both a reference site correction and long-period ocean variability correction using OGCMs. Red circles indicate the locations of GNSS sites PAWA, CKID, MAHI, and MAKO. The subduction interface slow slip contours, in millimeters, of the 2014 SSE are shown in light blue (Wallace et al., 2016), in addition to the Hikurangi deformation front (in black; Barnes et al., 2018, 2010, 2020; Collot et al., 2001; Crutchley et al., 2020).

POBS18-3 (see Figure 9). The temporal similarity of the signals suggests that the seafloor pressure signal may reflect SSE-related uplift; however, a signal is not present at the seafloor sensors closer to PAWA, and we observe almost no overall offset across this short period at POBS18-3 and LBPR18-4 (Figure 8), making it challenging to estimate potential vertical displacement. None of the OGCMs predict a relative pressure change (between the APG/POBS sites and reference site) similar to the observed signal; however, this doesn't exclude the possibility that the signal is oceanographic as such rapid variations due to small scale eddies are not likely to be modeled accurately by the global OGCMs. This highlights a need for higher resolution regional OGCMs, which may capture the short-term ocean variations better and improve the detection threshold of rapidly evolving slow slip events.

4.2. Offshore Gisborne Vertical Displacement

The closest onshore GNSS station to the offshore Gisborne pressure sensors is at Makorori Station (MAKO; Figure 9) and it experienced a burst of eastward motion at the end of March 2019 for approximately 1 week, followed by more gradual eastward motion until the end of April (Figure 8). Due to large amplitude oceanographic fluctuations recorded by the pressure sensors after 1 July, we exclude APG data after this time from our interpretation of tectonic activity offshore Gisborne. A positive offset in equivalent vertical displacement is estimated at all offshore Gisborne APGs over the period of the SSE; however, the APG data lack resolution to differentiate whether this occurred at the same time as the late-March eastward burst at MAKO. After full processing, these offsets are 1.4 ± 0.8 cm at U1519, 2.1 ± 0.7 cm at KU18-4, 3.0 ± 0.6 cm at KU18-3, 3.3 ± 0.4 cm at KU18-2, and 1.0 ± 0.3 cm at U1518. The APGs involve smaller estimated uplift values when the long-period ocean variability

is not applied: 0.4 ± 0.7 cm, 1.1 ± 0.7 cm, 2.2 ± 0.6 cm, 2.2 ± 0.5 cm, and 0.6 ± 0.4 cm for U1519, KU18-4, KU18-3, KU18-2, and U1518 respectively. This suggests that for the 2019 SSE period offshore Gisborne, the relative long-period ocean variability between the APGs and the reference site may act to mask some of the tectonic signal, leading to potential underestimation of equivalent vertical displacement if not accounted for.

Our study provides the second investigation of offshore vertical displacement due to a large, shallow SSE offshore Gisborne (the first being the 2014/2015 HOBITSS experiment). The pressure sensors deployed in the HOBITSS experiment covered a larger portion of the offshore Gisborne area (and at greater density) compared to the 2019 deployment (Wallace et al., 2016). Using pressure sensors from the HOBITSS experiment, Wallace et al. (2016) estimated 1.5–5.4 cm of seafloor uplift associated with the 2014 SSE. The 2019 APG network spans the northern edge of the 2014 SSE (see subduction interface slow slip contours in Figure 9). We note that the onshore GNSS displacements observed during the 2014 SSE involved up to ∼0.6 cm more subsidence, and up to 0.9 cm less eastward motion at the Gisborne coast than observed during the 2019 SSE, therefore some difference between uplift estimates is anticipated as there will be variations in the underlying slip distribution between the two events. The offshore Gisborne 2019 SSE displacement estimates presented here are 0.2–1.3 cm smaller at KU18–4, U1518, and U1519 and 1.9 and 0.1 cm larger at KU18-2 and KU18-3 respectively, than similarly located APGs in place during the 2014 SSE (Wallace et al., 2016). The 2014 APG that detected the largest uplift (5.4 cm) was located ∼20 km southwest of our 2019 array (above the 200 mm peak slip contour in Figure 9), so we don't expect or observe the same high vertical displacements that were estimated in 2014, as our 2019 APGs were not located above the locus of largest SSE slip. It should be noted that the coarse spacing between instruments in the 2019 seafloor deployment is a minimum for this area (and Hawke Bay). The coarse spacing makes interpreting the vertical displacement distribution more challenging, despite the more sophisticated pressure data processing sequence, than the previous HOBITSS experiment, which had a larger number of instruments with denser spacing.

5. Discussion

5.1. Value of Deploying Self-Calibrating Pressure Sensors

One of the challenges of processing and interpreting seafloor pressure data is the influence of sensor drift (Polster et al., 2009). For regular pressure sensor time series containing potential transient deformation signals, the periods of potential deformation should ideally be masked before the drift determination. The masking is required so that any vertical deformation during the transient deformation event is not absorbed into the instrument drift estimate. In some cases, this limits the periods of time that can be used to estimate drift rates, which may lead to less accurate drift corrections. A-0-A sensors enable independent calibration of the drift, greatly reducing any uncertainties in identifying tectonic signals and vertical displacement (assuming the reference site has been properly drift corrected and was situated at a location with a representative oceanic signal). If a limited number of A-0-A sensors are available, deploying them above the SSE area is preferable.

Keeping the period of data used for the offset calculation the same for the 2019 experiment data, we find a variation of 0.2–5.8 cm in the vertical displacement estimates when varying the period of data used in the estimation of drift of the regular APGs (see Table S4 in Supporting Information S1). Sensors equipped with self-calibration, such as the A-0-A approach, are not faced with the problem of tectonic or large amplitude ocean noise influencing the drift correction. Our study shows that sensors equipped with self-calibration allow for effective minimization of sensor drift, as shown in Figure 4, reducing the problem of unknown drift of seafloor sensors—as also demonstrated by Wilcock et al. (2021). Therefore, the range of displacement estimates we find for the regular pressure sensor data based on different drift correction periods (variations of 0.2–5.8 cm, Table S4 in Supporting Information S1) does not exist for the self-calibrated data.

Depending on the time period used for the estimation of drift of the LBPR18-4 (a regular APG) time series, a 0.8–3.3 cm range of vertical displacement estimates is obtained (see Figure 10). The LBPR18-4 and POBS18-3 pressure sensors were at 2,207 m and 1,930 m water depth respectively, located 22.5 km apart in the along-strike direction in the Hawke Bay array (Figure 9), and recorded similar pressure variations throughout the deployment (see reference site corrected time series data in Figures 8 and 10). The POBS18-3 time series can be used as a plausibility check to identify what time period may provide the most appropriate drift correction to LBPR18-4 (i.e., using pre-SSE data for the estimation of drift, Figure 10b), assuming that the major tectonic

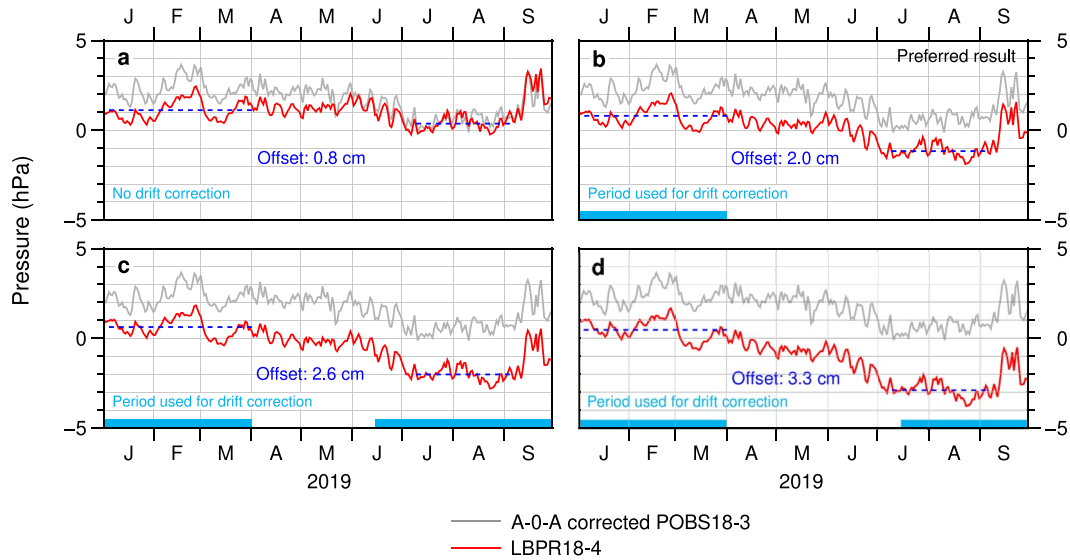

Figure 10. The LBPR18-4 and self-calibrated POBS18-3 pressure time series after reference site and long-period ocean variability corrections. The subplots indicate the difference in the LBPR18-4 time series (red) and offset over the SSE period (difference between dark blue dashes) when different periods are used to estimate drift (denoted with light blue bars). The self-calibrated POBS18-3 time series (gray) is identical in all subplots and is offset from the LBPR18-4 data by 1 hPa at 1 January 2019 for visualization purposes. Pressure is shown in hectopascals with the convention that an increase in the height of the water column is shown as a positive pressure change. (a) Before drift correction of LBPR18-4 data. (b) Using pre-SSE data for estimation of LBPR18-4 drift (the preferred drift correction, see Section 3.5). (c) Using data before and after the SSE for estimation of LBPR18-4 drift (SSE timing insight from GNSS site CKID data). (d) Using data before and after the SSE for estimation of LBPR18-4 drift (SSE timing insight from GNSS site CKID and POBS18-3 data).

and oceanographic features and trends of the two pressure sensor time series are similar. This demonstrates that equipping sensors with self-calibration such as A-0-A is not only valuable for minimizing the sensor drift of the equipped sensors but if the equipped sensor is deployed close to regular pressure sensors (<25 km spacing along similar isobaths), the self-calibrated data can be used to guide drift correction of the regular sensors.

The drift-corrected A-0-A pressure sensors were essential to demonstrating that some oceanographic trends remain in the data over longer time scales, even with the more effective ocean noise correction of a similar water depth reference site. The oceanographic trends are unlikely to follow the same rate and polarity throughout the deployment footprint, particularly for experiments longer than several months. If not accounted for, this oceanographic component could exaggerate or hide the SSE signal, impacting the quantification of vertical deformation during these transient events (Gomberg et al., 2019). The self-calibrating sensors in the 2019 experiment, deployed in the Hawke Bay area at 1,225–1,930 m depth, help justify the incorporation of long-period information from OGCMs into our analysis and interpretation. The largely drift-free A-0-A observations revealed similarities between the long-period predictions from the OGCMs and the reference site-corrected seafloor pressure data (Figure 7). Using a regional OGCM to reproduce ocean circulation in Monterey Bay, Wilcock et al. (2021) also identified long-period pressure variations in self-calibrated pressure data due to ocean variability signals.

When the long-period pressure variations predicted by the OGCMs are removed, our vertical displacement estimates are changed from −0.3–0.8 cm at the POBS sensors (without the correction), to 1.1–1.8 cm vertical displacement. Data from the seafloor sites are critical for determining the distribution and timing of the 2019 SSE activity, and therefore it is crucial that the sensor drift and ocean noise components are optimally removed; otherwise, the vertical displacement estimates can lead to misleading interpretations and modeling of SSE activity. After testing the long-period ocean variability correction for the self-calibrated data, the need for a relative long-period ocean variability correction is clear, and is used for the other Hawke Bay sensors (GNS18-3 and LBPR18-4), and the Gisborne array APGs, although the OGCM seafloor pressure predictions for the Gisborne region are unable to be verified with self-calibrated data.

5.2. Selecting an Effective Reference Site

We reiterate the proposition of Fredrickson et al. (2019), that seafloor pressure sensors should be deployed with reference sites located on similar isobaths to the main array (i.e., "depth matched sites"). For the Hawke Bay array in our study, the depth matched pressure sensor (GNS18-7) provided a more effective common-mode noise reduction than the deep reference sites (Figures 5 and 6) located 20–60 km away from the array. However, the depth matched pressure sensor is located too far (~180 km along-strike) from the APGs overlying the Gisborne SSE region to reduce ocean noise more effectively than the nearer deep-water site. Sub-regional variability in oceanographic signals may arise due to complex bathymetric features, such as canyons, lying between the reference and main array sites, and localized interactions between currents and eddies.

Our comparison of the reference-site-corrected observed pressure with predicted seafloor pressure from OGCMs (Figure 7 and Figures S3–S12 in Supporting Information S1) shows that APG/POBS and reference site localities, separated by 15–90 km, experience slightly different long-period oceanographic variations, even when placed at similar water depths. The difference in long-period ocean variability between reference sites and main array APGs is likely due to changes in character and migration of the major currents and eddies offshore North Island. This indicates that for reference site depth-matching to be effective, seafloor experiments need to be designed with consideration to the broad-scale bathymetric features and local circulation specifics. Attempting to correct for the remaining long-period differences in the 2019 deployment pressure data, using global OGCMs ECCO2, GLORYS, and HYCOM (with corrections scaled by a correlation coefficient), results in up to a 2.6 cm difference in vertical displacement estimates compared to those using reference sites only, suggesting that vertical displacement estimates of data without this additional oceanographic correction (i.e., only applying the common-mode noise correction using reference sites) may be influenced by oceanographic signals on the order of a few centimeters.

5.3. Performance of OGCMs in Simulating Seafloor Pressure

All three OGCMs used in this study are multi-layered, baroclinic, global models, with varying horizontal resolution: 1/4° for ECCO2, and 1/12° for GLORYS and HYCOM (Figure S17 in Supporting Information S1). The density of site spacing has implications for the use of these three OGCMs. ECCO2 has coarser resolution than the other two global OGCMs, and for the 2019 deployment, in some cases, multiple APG sites were located in the same ECCO2 grid cell. While ECCO2 appears to produce sensible pressure predictions relative to the other models that contain higher spatial resolution (HYCOM and GLORYS), it is important to be aware of the coarser horizontal resolution of ECCO2, which could make it difficult to use for investigating relative pressure variations in denser seafloor pressure arrays. This may also be applicable to GLORYS and HYCOM for the more closely spaced Gisborne array, as the horizontal resolution of these models is comparable to the sensor spacing for the 2019 experiment.

In order to incorporate bottom pressure predictions from OGCMs in the processing of pressure data from future seafloor experiments, both at the Hikurangi subduction zone and elsewhere, regional OGCMs (e.g., Regional Ocean Modeling System based configurations with higher horizontal resolution) may be preferable. The higher horizontal resolution could allow regional OGCMs to better capture the recorded relative long-period ocean variability between reference sites and main arrays APGs. However, in general OGCMs (both global and regional) are not optimized for determining bottom pressure and do not contain many pressure observation constraints. Even with the higher resolution of 1/12°, global OGCMs struggle to capture the complexities of New Zealand ocean circulation due to a relatively narrow continental shelf, high variability in climate, and the smoothing of complex bathymetric features (e.g., canyons, Figure 2; de Souza et al., 2020). Despite this, in our study, we observe that global OGCMs can still provide general guidance about potential regional long-period seafloor pressure trends due to variations in density, currents, and eddies. This may then be used to inform decisions about which global OGCM should be used as boundary conditions for a high resolution regional OGCM.

Ocean reanalysis products (which use a larger array of data sets) are preferable over non-assimilative ocean models and have been proven to reproduce the large scale flows around New Zealand with a reasonable degree of fidelity (de Souza et al., 2020). However, these products tend to lag present-day observations by a few years. Repeating our investigation using a regional OGCM, driven at its boundaries by an ocean reanalysis product, would be worthwhile. A regional OGCM has been previously tested by Gomberg et al. (2019) using pressure data

recorded during the 2014 HOBITSS experiment, where they suggest that the 2014 SSE-related displacement estimates calculated using only the reference site method might contain a component due to oceanographic signals. However, no self-calibrated (drift-corrected) pressure data were available during that experiment, limiting the ability to assess OGCM performance for the longer period signals recorded in 2014 and potential incorporation of the regional OGCM into the pressure processing in the way that we suggest here.

Comparison of the self-calibrated POBS data and simulated seafloor pressure using global OGCMs for the data corrected with reference sites (relative pressure variations, Figure 7), indicates that the OGCMs may be capable of reproducing pressure variations associated with long-term ocean variability. No OGCM was clearly identified as outperforming the others, and each captures different features of the observed data. The viability of the long-period ocean variability correction we use in this paper depends on the accuracy of the OGCM pressure simulations for each APG/POBS site and was assessed to some extent against the calibrated pressure data (without sensor drift). If the OGCMs do not reproduce the long-period ocean variability well, then applying the additional correction risks introducing anomalous signals into the observed data, impacting the interpretation of transient deformation events.

We recommend that geodetic studies test multiple OGCMs to assess which features of the bottom pressure simulations are robust when applying corrections incorporating OGCMs, rather than relying on the accuracy of a single OGCM. The accuracy of the OGCM bottom pressure simulations is unknown and varies depending on which OGCM is used and even within a single OGCM (spatially and temporally). This is demonstrated by the variety of trends predicted by different models for single seafloor sites and the same model for multiple sites (Figure 7 and Figures S3–S12 in Supporting Information S1), and the span of vertical displacement estimates at each site from 1.2 to 6.8 cm when using corrections based on the different OGCMs independently (Figures S18 and S19 in Supporting Information S1).

5.4. Independent Constraints to Assist Detecting Vertical Deformation

For seafloor pressure experiments aiming to detect vertical deformation, having access to independent measures of tectonic deformation (in addition to pressure sensor data) is highly advantageous, both to confirm the timing of SSEs and to provide additional, complementary information on the SSE evolution. We are fortunate in New Zealand that the onshore GNSS network is relatively close to the shallow plate boundary (the plate interface is only 12–15 km beneath the coastline), such that SSEs <15 km depth are typically detected by GNSS sites. However, for most subduction zones (like Cascadia and northern Japan, where the equivalent shallow portion of the plate boundary is >50–100 km offshore) onshore GNSS networks are too far from the shallow plate interface to detect similar SSEs. The GNSS network in New Zealand provides important information about the timing and along-strike distribution of slip near the coast. To gain resolution offshore, of New Zealand and elsewhere, GNSS-Acoustic arrays (Bürgmann & Chadwell, 2014) could be used to constrain horizontal deformation during SSEs, if surveyed frequently enough, and if the SSEs are large enough (e.g., Yokota & Ishikawa, 2020). Formation pressure changes measured by IODP observatories (as a proxy for volumetric strain) can provide excellent temporal resolution of transient deformation, as demonstrated by Araki et al. (2017) and Davis et al. (2015) at the Nankai subduction zone and Costa Rica's Middle America Trench, respectively. If seafloor pressure sensors are located near such observatories, then key information about the onset and migration of slow slip would be available to enhance resolution of the slow slip processes. Given the high-noise seafloor environment, multiple proxies in addition to seafloor pressure (e.g., onshore GNSS, seismological evidence for tectonic tremor, GNSS-Acoustic measurements, and/or borehole pressure sensing) are needed to confidently assess whether seafloor pressure changes are tectonic or oceanographic in origin.

The vertical displacements from seafloor pressure sensor data are often the only data constraining the distribution and magnitude of offshore slow slip, particularly for most subduction zones where the shallow plate boundary is far from the nearest onshore GNSS stations. Over- or under-estimated seafloor displacements would therefore contribute significant error to any slip models of SSE along shallow subduction interfaces. It is critical that the oceanographic noise is accounted for as thoroughly as possible in order to accurately estimate the vertical displacement of the seafloor. Watts et al. (2021) propose that deploying Current meters and bottom Pressure recording Inverted Echo Sounders (CPIES) can enable an effective empirical technique for reducing oceanographic noise and revealing periods of vertical deformation. They find that combining seafloor pressure and near-bottom current measurements with optimal interpolation is successful at reducing ocean noise and

revealing seafloor displacement for recorded CPIES data offshore Oregon, USA, when applied to simulated slow slip signals, but this is yet to be tested for a recorded SSE. It is clear that the key to reducing the oceanographic component of pressure data requires improved knowledge of the oceanographic variations in the region of seafloor pressure deployment, in addition to, or instead of, locally deployed reference sites. It is strongly encouraged that future seafloor experiments be designed with contributions from multiple disciplines—involving collaboration among seafloor geodesists, physical oceanographers, and ocean circulation modelers.

6. Conclusion

Seafloor pressure sensors often provide the only observations constraining crustal deformation caused by offshore, shallow subduction zone slow slip events. Correcting seafloor pressure data for ocean noise and sensor drift, with the intention of resolving centimeter-level tectonic displacements, can lead to misinterpretation of tectonic deformation if the data are not processed carefully. Using seafloor pressure data from a 2019 experiment at the Hikurangi subduction zone, we estimate the vertical displacement of the seafloor resulting from a large SSE beneath the array during March–June 2019. The deployment included three sensors with A-0-A (ambient-zero-ambient) self-calibration systems, which were effective at reducing residual linear trends of the two gauges of each sensor to within 0.7–2.5 hPa/yr of each other (equivalent to 0.06–0.2 cm change in water depth per month). This independent removal of drift allowed us to compare the time series with seafloor pressure simulations from multiple global OGCMs. This showed that although the short-period oceanographic changes were not well-predicted by the OGCMs, the longer period (>90 days), relative oceanographic variations (between APGs and a locally deployed reference site) were predicted well by some OGCMs. This prompted us to use the reference site for initial common-mode ocean noise removal, and then the simulated data from OGCMs to correct for remaining long-period oceanographic variations.

We show that the long-period correction has a significant influence on most of our SSE vertical displacement estimates: decreasing uplift estimated from the APG data for two sites (by 0.6 and 2.6 cm) and increasing uplift estimates for eight sites (by 0.3–1.6 cm). During the 2019 SSE, we calculate 1.0–3.3 cm of uplift off Gisborne at the northern Hikurangi subduction zone, and 1.1–2.7 cm of uplift in Hawke Bay off central Hikurangi. Some displacements in Hawke Bay appeared delayed by 6 weeks compared to the onset of SSE-related motion onshore, suggesting updip migration of the SSE, although future, denser (<10–15 km site spacing) deployments during SSEs beneath Hawke Bay are needed to confirm this SSE behavior. Based on our analysis of the 2019 pressure data, we recommend that future seafloor pressure sensor experiments targeting SSEs should be designed with consideration to the broad-scale bathymetric features and local circulation characteristics to give an impression of the uncertainty regarding the drift of the A-0-A instrument. It is highly advantageous for seafloor investigations to include self-calibrating pressure sensors, depth matched reference sites, and insight from independent indicators of transient deformation events (e.g., with nearby onshore GNSS stations, seafloor GNSS-A surveys and borehole pressure sensing) and oceanographic variations (e.g., using OGCMs and ocean bottom current meters).

Data Availability Statement

Seafloor pressure data from the APGs/POBSs used in this study are publicly available at https://doi.org/10.5281/zenodo.5834879. GeoNet GNSS data are available from www.geonet.org.nz. The OGCMs used can be sourced from https://ecco-group.org/products.htm for ECCO2, GLOBAL_REANALYSIS_PHY_001_030 from https://data.marine.copernicus.eu/product for GLORYS, and https://tds.hycom.org/thredds/catalogs/GLBv0.08/expt_93.0.html for HYCOM. Pressure data were processed using MATLAB (ver R2019b and ver R2021b), and figures were generated using Generic Mapping Tools (GMT 6; Wessel et al., 2013).

Acknowledgments
This project was supported by an Endeavour research grant from the New Zealand Ministry for Business, Innovation, and Employment (MBIE; funding contract C05X1605), NSF grant OCE-1754929, and the Ministry of Education, Culture, Sports, Science and Technology (MEXT) of Japan, under its The Second Earthquake and Volcano Hazards Observation and Research Program (Earthquake and Volcano Hazard Reduction Research). The first author was also partly supported by a VUW Doctoral Scholarship. We thank Carlos Becceril, Ted Koczynski, Pete Liljegren, Merijn Thornton, Syuichi Suzuki, Tomohiro Inoue, Motoyuki Kido, Soli Garcia, and Will Quinn for contributions to instrument deployment and recoveries. We also thank the captains and crews of the R/V Tangaroa and R/V Roger Revelle and onboard science parties of voyages TAN1809, RR1903, and TAN1908. We gratefully acknowledge ship time on R/V Tangaroa which made this work possible, funded by New Zealand MBIE and administered by the Tangaroa Reference Group. We also acknowledge the New Zealand GeoNet project and its sponsors EQC, GNS Science and LINZ, for providing GNSS data used in this study. We thank the Associate Editor, reviewer Erik Fredrickson, and one anonymous reviewer, for providing useful feedback which helped improve the manuscript. Open access publishing facilitated by Victoria University of Wellington, as part of the Wiley - Victoria University of Wellington agreement via the Council of Australian University Librarians.

References

Androsov, A., Boebel, O., Schröter, J., Danilov, S., Macrander, A., & Ivanciu, I. (2020). Ocean bottom pressure variability: Can it be reliably modeled? *Journal of Geophysical Research: Oceans*, *125*(3). https://doi.org/10.1029/2019JC015469

Araki, E., Saffer, D. M., Kopf, A. J., Wallace, L. M., Kimura, T., Machida, Y., et al. (2017). Recurring and triggered slow-slip events near the trench at the Nankai Trough subduction megathrust. *Science*, *356*(6343), 1157–1160. https://doi.org/10.1126/science.aan3120

Avouac, J. P. (2015). From geodetic imaging of seismic and aseismic fault slip to dynamic modeling of the seismic cycle. *Annual Review of Earth and Planetary Sciences*, *43*(1), 233–271. https://doi.org/10.1146/annurev-earth-060614-105302

Barker, D. H. N., Wallace, L. M., Woods, K., Savage, M. K., & TAN1809 Science Party. (2019). Hikurangi Ocean Bottom Investigation of Tremor and Slow Slip (HOBITSS V). https://doi.org/10.21420/Z4FK-SK46

Barnes, P. M., Ghisetti, F. C., Ellis, S., & Morgan, J. K. (2018). The role of protothrusts in frontal accretion and accommodation of plate convergence, Hikurangi subduction margin, New Zealand. *Geosphere*, *14*(2), 440–468. https://doi.org/10.1130/GES01552.1

Barnes, P. M., Lamarche, G., Bialas, J., Henrys, S., Pecher, I., Netzeband, G. L., et al. (2010). Tectonic and geological framework for gas hydrates and cold seeps on the Hikurangi subduction margin, New Zealand. *Marine Geology*, *272*(1–4), 26–48. https://doi.org/10.1016/j.margeo.2009.03.012

Barnes, P. M., Wallace, L. M., Saffer, D. M., Bell, R. E., Underwood, M. B., Fagereng, A., et al. (2020). Slow slip source characterized by lithological and geometric heterogeneity. *Science Advances*, *6*(13). https://doi.org/10.1126/sciadv.aay3314

Bartlow, N. M., Wallace, L. M., Beavan, R. J., Bannister, S., & Segall, P. (2014). Time-dependent modeling of slow slip events and associated seismicity and tremor at the Hikurangi subduction zone, New Zealand. *Journal of Geophysical Research: Solid Earth*, *119*(1), 734–753. https://doi.org/10.1002/2013JB010609

Beavan, J., Tregoning, P., Bevis, M., Kato, T., & Meertens, C. (2002). Motion and rigidity of the Pacific Plate and implications for plate boundary deformation. *Journal of Geophysical Research*, *107*(B10), ETG 19-1–ETG 19-15. https://doi.org/10.1029/2001jb000282

Bürgmann, R. (2018). The geophysics, geology and mechanics of slow fault slip. *Earth and Planetary Science Letters*, *495*, 112–134. https://doi.org/10.1016/j.epsl.2018.04.062

Bürgmann, R., & Chadwell, D. (2014). Seafloor geodesy. *Annual Review of Earth and Planetary Sciences*, *42*(1), 509–534. https://doi.org/10.1146/annurev-earth-060313-054953

Chiswell, S. M. (2005). Mean and variability in the Wairarapa and Hikurangi eddies, New Zealand. *New Zealand Journal of Marine & Freshwater Research*, *39*(1), 121–134. https://doi.org/10.1080/00288330.2005.9517295

Chiswell, S. M., Bostock, H. C., Sutton, P. J. H., & Williams, M. J. (2015). Physical oceanography of the deep seas around New Zealand: A review. *New Zealand Journal of Marine & Freshwater Research*, *49*(2), 286–317. https://doi.org/10.1080/00288330.2014.992918

Clark, K., Howarth, J., Litchfield, N., Cochran, U., Turnball, J., Dowling, L., et al. (2019). Geological evidence for past large earthquakes and tsunamis along the Hikurangi subduction margin, New Zealand. *Marine Geology*, *412*, 139–172. https://doi.org/10.1016/j.margeo.2019.03.004

Cochran, U., Berryman, K., Zachariasen, J., Mildenhall, D., Hayward, B., Southall, K., et al. (2006). Paleoecological insights into subduction zone earthquake occurrence, eastern North Island, New Zealand. *Bulletin of the Geological Society of America*, *118*(9–10), 1051–1074. https://doi.org/10.1130/B25761.1

Collot, J. Y., Lewis, K., Lamarche, G., & Lallemand, S. (2001). The giant Ruatoria debris avalanche on the northern Hikurangi margin, New Zealand: Result of oblique seamount subduction. *Journal of Geophysical Research*, *106*(B9), 19271–19297. https://doi.org/10.1029/2001jb900004

Crutchley, G. J., Klaeschen, D., Henrys, S. A., Pecher, I. A., Mountjoy, J. J., & Woelz, S. (2020). Subducted sediments, upper-plate deformation and dewatering at New Zealand's southern Hikurangi subduction margin. *Earth and Planetary Science Letters*, *530*, 115945. https://doi.org/10.1016/j.epsl.2019.115945

Cummings, J. A. (2006). Operational multivariate ocean data assimilation. *Quarterly Journal of the Royal Meteorological Society*, *131*(613), 3583–3604. https://doi.org/10.1256/qj.05.105

Cummings, J. A., & Smedstad, O. M. (2013). Variational data assimilation for the global ocean. In *Data assimilation for atmospheric, oceanic and hydrologic applications* (Vol. 2, pp. 303–343). Springer. https://doi.org/10.1007/978-3-642-35088-7_13

Davis, E. E., Villinger, H., & Sun, T. (2015). Slow and delayed deformation and uplift of the outermost subduction prism following ETS and seismogenic slip events beneath Nicoya Peninsula, Costa Rica. *Earth and Planetary Science Letters*, *410*, 117–127. https://doi.org/10.1016/j.epsl.2014.11.015

de Souza, J. M. A. C., Couto, P., Soutelino, R., & Roughan, M. (2020). Evaluation of four global ocean reanalysis products for New Zealand waters—A guide for regional ocean modelling. *New Zealand Journal of Marine & Freshwater Research*, *55*(1), 132–155. https://doi.org/10.1080/00288330.2020.1713179

Dobashi, Y., & Inazu, D. (2021). Improving detectability of seafloor deformation from bottom pressure observations using numerical ocean models. *Frontiers in Earth Science*, *8*, 621. https://doi.org/10.3389/feart.2020.598270

Fox, C. G. (1990). Evidence of active ground deformation on the mid-ocean ridge: Axial Seamount, Juan de Fuca Ridge, April–June 1988. *Journal of Geophysical Research*, *95*(B8), 12813–12822. https://doi.org/10.1029/jb095ib08p12813

Fox, C. G. (1993). Five years of ground deformation monitoring on axial seamount using a bottom pressure recorder. *Geophysical Research Letters*, *20*(17), 1859–1862. https://doi.org/10.1029/93GL01216

Fredrickson, E. K., Wilcock, W. S. D., Schmidt, D. A., MacCready, P., Roland, E., Kurapov, A. L., et al. (2019). Optimizing sensor configurations for the detection of slow-slip earthquakes in seafloor pressure records, using the Cascadia subduction zone as a case study. *Journal of Geophysical Research: Solid Earth*, *124*(12), 13504–13531. https://doi.org/10.1029/2019JB018053

Gennerich, H. H., & Villinger, H. (2011). Deciphering the ocean bottom pressure variation in the Logatchev hydrothermal field at the eastern flank of the Mid-Atlantic Ridge. *Geochemistry, Geophysics, Geosystems*, *12*(7). https://doi.org/10.1029/2010GC003441

Gomberg, J., Hautala, S., Johnson, P., & Chiswell, S. (2019). Separating sea and slow slip signals on the seafloor. *Journal of Geophysical Research: Solid Earth*, *124*(12), 13486–13503. https://doi.org/10.1029/2019JB018285

Heesemann, M., Insua, T. L., Scherwath, M., Juniper, K. S., & Moran, K. (2014). Ocean networks Canada: From geohazards research laboratories to smart ocean systems. *Oceanography*, *27*(2), 151–153. https://doi.org/10.5670/oceanog.2014.50

Helber, R. W., Townsend, T. L., Barron, C. N., Dastugue, J. M., & Carnes, M. R. (2013). *Validation test report for the improved synthetic ocean profile (ISOP) system, Part I: Synthetic profile methods and algorithm*. Naval Research Lab Stennis Detachment Stennis Space Center, MS Oceanography Division.

Inazu, D., Hino, R., & Fujimoto, H. (2012). A global barotropic ocean model driven by synoptic atmospheric disturbances for detecting seafloor vertical displacements from in situ ocean bottom pressure measurements. *Marine Geophysical Research*, *33*(2), 127–148. https://doi.org/10.1007/s11001-012-9151-7

Inoue, T., Ito, Y., Wallace, L. M., Yoshikawa, Y., Inazu, D., Garcia, E. S. M., et al. (2021). Water depth dependence of long-range correlation in nontidal variations in seafloor pressure. *Geophysical Research Letters*, *48*(8). https://doi.org/10.1029/2020gl092173

Ito, Y., Hino, R., Kido, M., Fujimoto, H., Osada, Y., Inazu, D., et al. (2013). Episodic slow slip events in the Japan subduction zone before the 2011 Tohoku-Oki earthquake. *Tectonophysics*, *600*, 14–26. https://doi.org/10.1016/j.tecto.2012.08.022

Ito, Y., Hino, R., Suzuki, S., & Kaneda, Y. (2015). Episodic tremor and slip near the Japan Trench prior to the 2011 Tohoku-Oki earthquake. *Geophysical Research Letters*, *42*(6), 1725–1731. https://doi.org/10.1002/2014GL062986

Kaneda, Y. (2014). A real-time monitoring system for megathrust earthquakes and tsunamis around southwestern Japan. *Oceanography*, *27*(2), 103–103. https://doi.org/10.5670/oceanog.2014.45

Kato, A., Obara, K., Igarashi, T., Tsuruoka, H., Nakagawa, S., & Hirata, N. (2012). Propagation of slow slip leading up to the 2011 Mw 9.0 Tohoku-Oki earthquake. *Science*, *335*(6069), 705–708. https://doi.org/10.1126/science.1215141

Kawaguchi, K., Kaneko, S., Nishida, T., & Komine, T. (2015). Construction of the DONET real-time seafloor observatory for earthquakes and tsunami monitoring. In *Seafloor observatories: A new vision of the Earth from the abyss* (pp. 211–228). Springer. https://doi.org/10.1007/978-3-642-11374-1_10

Lellouche, J. M., Greiner, E., Bourdallé-Badie, R., Garric, G., Melet, A., Drévillon, M., et al. (2021). The Copernicus global 1/12° oceanic and sea ice GLORYS12 reanalysis. *Frontiers in Earth Science*, *9*, 585. https://doi.org/10.3389/feart.2021.698876

Matsumoto, H., & Araki, E. (2021). Drift characteristics of DONET pressure sensors determined from in-situ and experimental measurements. *Frontiers in Earth Science*, *614*. https://doi.org/10.3389/feart.2020.600966

Menemenlis, D., Campin, J. M., Heimbach, P., Hill, C. N., Lee, T., Nguyen, A. T., et al. (2008). ECCO2: High resolution global ocean and sea ice data synthesis. *Mercator Ocean Quarterly Newsletter*, *31*, 13–21.

Mochizuki, M., Uehira, K., Kanazawa, T., Kunugi, T., Shiomi, K., Aoi, S., et al. (2018). S-net project: Performance of a large-scale seafloor observation network for preventing and reducing seismic and tsunami disasters. In *2018 OCEANS-MTS/IEEE Kobe Techno-Oceans (OTO)* (pp. 1–4). IEEE. https://doi.org/10.1109/OCEANSKOBE.2018.8558823

Mortimer, N., & Parkinson, D. (1996). Hikurangi Plateau: A Cretaceous large igneous province in the southwest Pacific Ocean. *Journal of Geophysical Research*, *101*(B1), 687–696. https://doi.org/10.1029/95JB03037

Muramoto, T., Ito, Y., Inazu, D., Wallace, L. M., Hino, R., Suzuki, S., et al. (2019). Seafloor crustal deformation on ocean bottom pressure records with nontidal variability corrections: Application to Hikurangi margin, New Zealand. *Geophysical Research Letters*, *46*(1), 303–310. https://doi.org/10.1029/2018GL080830

Pizer, C., Clark, K., Howarth, J., Garrett, E., Wang, X., Rhoades, D., & Woodroffe, S. (2021). Paleotsunamis on the southern Hikurangi subduction zone, New Zealand, show regular recurrence of large subduction earthquakes. *The Seismic Record*, *1*(2), 75–84. https://doi.org/10.1785/0320210012

Polster, A., Fabian, M., & Villinger, H. (2009). Effective resolution and drift of paroscientific pressure sensors derived from long-term seafloor measurements. *Geochemistry, Geophysics, Geosystems*, *10*(8). https://doi.org/10.1029/2009GC002532

Radiguet, M., Perfettini, H., Cotte, N., Gualandi, A., Valette, B., Kostoglodov, V., et al. (2016). Triggering of the 2014 Mw 7.3 Papanoa earthquake by a slow slip event in Guerrero, Mexico. *Nature Geoscience*, *9*(11), 829–833. https://doi.org/10.1038/ngeo2817

Ruiz, S., Metois, M., Fuenzalida, A., Ruiz, J., Leyton, F., Grandin, R., et al. (2014). Intense foreshocks and a slow slip event preceded the 2014 Iquique Mw 8.1 earthquake. *Science*, *345*(6201), 1165–1169. https://doi.org/10.1126/science.1256074

Saffer, D. M., & Wallace, L. M. (2015). The frictional, hydrologic, metamorphic and thermal habitat of shallow slow earthquakes. *Nature Geoscience*, *8*(8), 594–600. https://doi.org/10.1038/NGEO2490

Saffer, D. M., Wallace, L. M., Barnes, P. M., Pecher, I. A., Petronotis, K. E., LeVay, L. J., et al. (2019). Expedition 372B/375 summary. *Proceedings of the International Ocean Discovery Program*, *372*, 1–35. https://doi.org/10.14379/iodp.proc.372B375.101.2019

Sasagawa, G. S., Zumberge, M. A., & Cook, M. J. (2018). Laboratory simulation and measurement of instrument drift in quartz-resonant pressure gauges. *IEEE Access*, *6*, 57334–57340. https://doi.org/10.1109/ACCESS.2018.2873479

Schwartz, S. Y., & Rokosky, J. M. (2007). Slow slip events and seismic tremor at circum-Pacific subduction zones. *Review of Geophysics*, *45*(3). https://doi.org/10.1029/2006RG000208

Smith, W. H. F., & Sandwell, D. T. (1997). Global sea floor topography from satellite altimetry and ship depth soundings. *Science*, *277*(5334), 1956–1962. https://doi.org/10.1126/science.277.5334.1956

Wallace, L. M. (2020). Slow slip events in New Zealand. *Annual Review of Earth and Planetary Sciences*, *48*(1), 175–203. https://doi.org/10.1146/annurev-earth-071719-055104

Wallace, L. M., & Beavan, J. (2010). Diverse slow slip behavior at the Hikurangi subduction margin, New Zealand. *Journal of Geophysical Research*, *115*(B12), B12402. https://doi.org/10.1029/2010JB007717

Wallace, L. M., Beavan, J., Bannister, S., & Williams, C. (2012). Simultaneous long-term and short-term slow slip events at the Hikurangi subduction margin, New Zealand: Implications for processes that control slow slip event occurrence, duration, and migration. *Journal of Geophysical Research*, *117*(B11). https://doi.org/10.1029/2012JB009489

Wallace, L. M., Webb, S. C., Ito, Y., Mochizuki, K., Hino, R., Henrys, S., et al. (2016). Slow slip near the trench at the Hikurangi subduction zone, New Zealand. *Science*, *352*(6286), 701–704. https://doi.org/10.1126/science.aaf2349

Watts, D. R., Wei, M., Tracey, K. L., Donohue, K. A., & He, B. (2021). Seafloor geodetic pressure measurements to detect shallow slow slip events: Methods to remove contributions from Ocean water. *Journal of Geophysical Research: Solid Earth*, *126*(4). https://doi.org/10.1029/2020jb020065

Wessel, P., Smith, W. H., Scharroo, R., Luis, J., & Wobbe, F. (2013). Generic mapping tools: Improved version released. *Eos, Transactions American Geophysical Union*, *94*(45), 409–410. https://doi.org/10.1002/2013EO450001

Wilcock, W. S. D., Manalang, D. A., Fredrickson, E. K., Harrington, M. J., Cram, G., Tilley, J., et al. (2021). A thirty-month seafloor test of the A-0-A method for calibrating pressure gauges. *Frontiers in Earth Science*, *8*, 653. https://doi.org/10.3389/feart.2020.600671

Williams, C. A., Eberhart-Phillips, D., Bannister, S., Barker, D. H. N., Henrys, S., Reyners, M., & Sutherland, R. (2013). Revised interface geometry for the Hikurangi subduction zone, New Zealand. *Seismological Research Letters*, *84*(6), 1066–1073. https://doi.org/10.1785/0220130035

Williamson, A. L., & Newman, A. V. (2018). Limitations of the resolvability of finite-fault models using static land-based geodesy and open-ocean tsunami waveforms. *Journal of Geophysical Research: Solid Earth*, *123*(10), 9033–9048. https://doi.org/10.1029/2018JB016091

Yokota, Y., & Ishikawa, T. (2020). Shallow slow slip events along the Nankai Trough detected by GNSS-A. *Science Advances*, *6*(3), eaay5786. https://doi.org/10.1126/sciadv.aay5786